

A review of optical snow cover algorithms



Note no

SAMBA/40/06

Authors

Rune Solberg, Hans Koren and Jostein Amlien

Date

15 December 2006

Norsk Regnesentral

Norsk Regnesentral (Norwegian Computing Center, NR) is a private, independent, non-profit foundation established in 1952. NR carries out contract research and development projects in the areas of information and communication technology and applied statistical modeling. The clients are a broad range of industrial, commercial and public service organizations in the national as well as the international market. Our scientific and technical capabilities are further developed in co-operation with The Research Council of Norway and key customers. The results of our projects may take the form of reports, software, prototypes, and short courses. A proof of the confidence and appreciation our clients have for us is given by the fact that most of our new contracts are signed with previous customers.

Title	A review of optical snow algorithms
Authors	Rune Solberg, Hans Koren and Jostein Amlien
Date	15 December 2006
Year	2006
Publication number	SAMBA/40/06

Abstract

The purpose of this report is to provide a review of optical snow cover algorithms to assist algorithm selection in the CryoRisk project. The first part of the report provides a brief review of the state of the art for snow cover retrieval algorithms developed internationally. The review covers classification algorithms (snow/non-snow algorithms), fractional snow cover algorithms (snow fraction per pixel) and multi-sensor algorithms. The report then goes into more details for algorithms developed and refined nationally by describing the algorithms, presenting results from algorithm evaluation and then discussing the evaluation results. The algorithms covered are the Norwegian-Linear-Reflectance-to-snow-cover (NLR) algorithm, NR's cloud detection algorithm, NR's new fractional snow cover algorithm and a multi-sensor time-series algorithm combining optical and synthetic aperture radar data. The algorithms and evaluations presented build on results from many projects carried out over a period of about ten years. The motivation for the national focus is that quite a lot of resources have been invested in research and development for snow cover retrieval algorithms in Norway, and it is then logical to build on this experience when developing an operational service. The last chapter provides recommendations for a process leading to operationalisation of algorithms in the CryoRisk project.

Keywords	Remote sensing, snow cover area
Target group	NVE
Availability	Open
Project number	220 286
Research field	Remote sensing
Number of pages	66
© Copyright	Norsk Regnesentral

Contents

1	Introduction.....	7
2	A brief review of the state of the art for optical snow algorithms	8
2.1	Classification algorithms.....	8
2.2	Fractional snow cover retrieval.....	10
2.3	Multi-sensor snow cover retrieval.....	13
3	NR's optical snow algorithms	15
3.1	The NLR snow algorithm.....	15
3.1.1	The algorithm in detail.....	15
3.1.2	Processing flow	17
3.2	Cloud detection in the presence of snow	19
3.3	NR's new optical snow model algorithm	22
3.3.1	Spectral BRDF model grid	22
3.3.2	Assimilation algorithm	24
3.3.3	Metamorphosis and impurity projection	25
3.3.4	Fractional snow cover algorithm	26
3.4	Multi-sensor time-series snow cover algorithm.....	28
3.4.1	Baseline algorithm	28
3.4.2	Day-product approach	30
4	Evaluation of NR's optical snow algorithms	31
4.1	The NLR algorithm	31
4.1.1	Data set.....	31
4.1.2	Snow classification.....	34
4.1.3	Results	36
4.2	The cloud detection algorithm	44
4.3	NR's new optical snow model algorithm	46
4.3.1	Validation approach	46
4.3.2	First experimental results.....	46
4.4	The multi-sensor time-series snow cover algorithm.....	49

5	Discussion of results	54
5.1	The NLR algorithm	54
5.2	The cloud detection algorithm	56
5.3	NR's new optical snow model algorithm	57
5.4	Multi-sensor time-series snow cover algorithm	58
6	Overall conclusions and recommendations	60
6.1	Norwegian algorithms	60
6.2	Other algorithms	61
6.3	Operationalisation scenarios	62
7	References	64

1 Introduction

Monitoring seasonal snow cover is important for several purposes. In northern regions, the snow may represent more than half the annual runoff, putting specific demands on the models and other tools employed in managing this water resource. Risk of flooding increases this demand, both in areas with stable winter snow cover, and in areas only occasionally covered with snow. Snow covered ground affects the energy exchange processes developing weather and climate, both locally and in large regions, and is an important element in meteorological modelling tools. The snow pack itself causes avalanches every year in alpine regions, enforces a high-priority road-clearing service both in cities and in rural areas, and affects many other aspects of human life.

Operational snow cover area mapping by optical sensors has taken place for more than two decades, but there is still a demand for improved accuracy. Most operational products are binary (snow/non-snow). Since snow cover is a rapidly changing phenomenon in many regions, there is a need for frequent mapping. To achieve frequent mapping sensors with medium to low spatial resolution have to be used. Thus, to achieve the details required in many applications, fractional snow cover area mapping is needed. Therefore, Norway has for a long time focussed on algorithms retrieving fractional snow cover.

The purpose of this report is to provide a review of optical snow cover algorithms to assist algorithm selection in the CryoRisk project, a Norwegian national project led by The Norwegian Water Resources and Energy Directorate (NVE) and The Norwegian Meteorological Institute (met.no). One of the aims of the CryoRisk project is to develop an operational snow cover monitoring and modelling service in Norway.

The first part of the report provides a brief review of the state of the art for snow cover retrieval algorithms developed internationally. The report then goes into more detail for algorithms developed and refined nationally by describing the algorithms, presenting results from algorithm evaluation and then discussing the evaluation results. Also a multi-sensor time-series algorithm combining optical and synthetic aperture radar data is presented as sensor fusion algorithms will be important in future applications. The algorithms and evaluations presented build on results from many projects carried out over a period of about ten years. The motivation for the national focus is that quite a lot of resources have been invested in research and development for snow cover retrieval algorithms in Norway, and it is then logical to build on this experience when developing an operational service.

2 A brief review of the state of the art for optical snow algorithms

Snow cover is the only snow parameter currently derived from optical data operationally. There has been and still is quite a lot of research performed to develop algorithms for accurate retrieval of the snow cover.

2.1 Classification algorithms

Most snow classification algorithms developed label snow into two classes only, "snow" and "no snow". This is usually sufficient for global and regional monitoring with low-resolution sensors (typically 1 km) and locally with high-resolution sensors (typically 30 meters). There are several published works where supervised classifiers have been used for the classification of snow cover, see e.g. Baumgartner and Rango (1995) and Swamy and Brivio (1996). The classifier is first trained using areas of known class. A statistical description is generated for each class using these areas (prototype classes are generated). Each pixel in the image is then classified according to the pixel's location in the multispectral space relative to the prototype classes. Various classifiers handles overlapping classes and the presence of prior information differently according to which classification rule is used. Common classification rules are Maximum Likelihood (ML) and Maximum A posteriori (MAP) (Ripley 1996). For the snow cover application the classes have to comprise snow and one or more bare-ground classes. Several bare ground classes are usually recommended to give the best discrimination from snow.

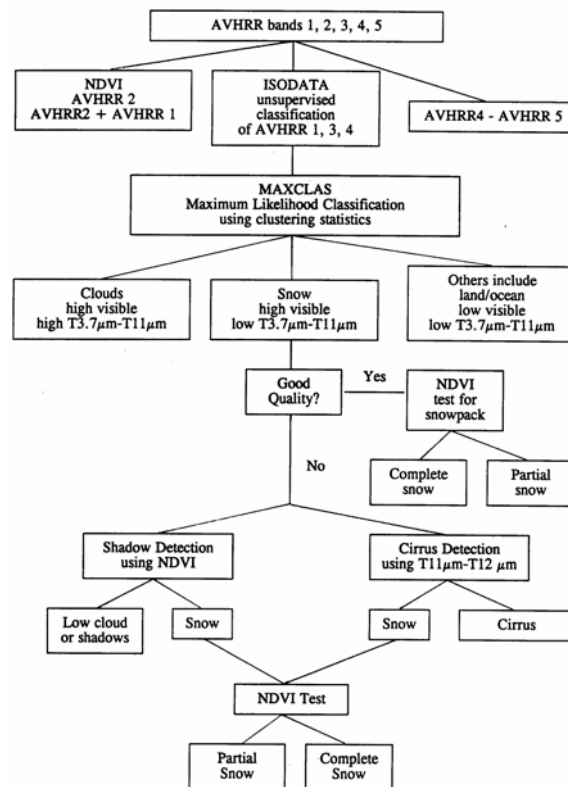


Figure 2.1. Flow diagram of a snow classification procedure for NOAA AVHRR imagery developed at University of Bristol including combined clustering (unsupervised classification) and the Maximum Likelihood classifier (supervised classification). (Bailey et al. 1993)

The main drawback of supervised classification is that prior information is necessary to define the training areas, and this requires manual intervention. Therefore, the main focus of research for development of snow classification methods has been towards automated methods. The approaches vary from hybrid supervised classification, where the training part is automated, to more physically related methods, which often corresponds to box classification of spectral and spectrally derived features.

A clustering algorithm divides the multi-spectral space into classes according to how the data is distributed. Several clustering algorithms are completely automatic. Harrison and Lucas (1989) have experimented with algorithms based on clustering (ISODATA) for classification of NOAA AVHRR imagery for snow cover mapping. Their experiments were mainly focused on the problem of how to discriminate between clouds and snow. This approach has been further improved as described in Xu et al. (1993), see Figure 2.1. The method combines the use of unsupervised and supervised classification. The ISODATA clustering algorithm is used to pre-classify the image based on AVHRR bands 1, 3 and 4. The clusters generated are used to determine a "signature" for each class present that is used for training of the supervised classifier. The Maximum Likelihood (ML) classifier is then used for the supervised classification.

Box classification approaches have been popular in remote sensing of snow because the methods are both automated and physically related. Detailed knowledge about the sensor and the physical properties of the classes is used to set threshold values that are used to partition the feature space. To enhance the separation of the natural clusters, new features are often made from arithmetic combinations of the bands. One such approach is proposed by Dozier (1989) for Landsat TM data. The following three criteria are used to discriminate snow from clouds or other bright sources:

1. The at-satellite planetary reflectance, R , in band 1 ($TM1$) must be above a certain threshold, t_{TM1} . Since $TM1$ usually is saturated for snow, the band is only usable for shaded areas where the threshold will distinguish snow from most other surfaces.
2. R_{TM5} has to be lower than a threshold t_{TM5} . This discriminates snow from most clouds.
3. The index $(R_{TM2} - R_{TM5}) / (R_{TM2} + R_{TM5})$, also called the Normalised Difference Snow Index (NDSI), has to be greater than a threshold t_{TM2-5} . The index helps discrimination of snow from bright soils and rocks and from clouds.

The optimal values for the thresholds are dependent on the atmospheric conditions. However, it is found that the algorithm is not dependent of very precise values for the thresholds, in particular not t_{TM1} and t_{TM5} . Dozier (1989) determined values of the thresholds for a particular Landsat TM image.

The experience from Landsat TM has been the foundation for the algorithm SNOWMAP developed for Terra MODIS (Riggs et al. 1994; Hall et al. 1995; Riggs et al. 1996). The algorithm works as follows:

1. The NDSI for MODIS $(R_{M4} - R_{M6}) / (R_{M4} + R_{M6})$ has to be greater than about 0.4, where $M4$ and $M6$ are MODIS bands 4 and 6. They are narrower but correspond otherwise to $TM2$ and $TM5$ which was used by Dozier (1989) described above. R is again the at-satellite planetary reflectance.

2. R_{M2} has to be greater than about 0.1.

The NDSI discriminates snow from most other bright sources, like clouds, soils and rocks (see Figure 2.2). Step 2 discriminates snow from water bodies, which is difficult to do with NDSI. Neither of the thresholds are very sensitive to their precise value. Hall et al. (1995) has found SNOWMAP very accurate (98%) for pixels with snow cover of more than 60%. It performed similar to supervised classification for cloud-free test scenes and better for cloudy scenes. The algorithm has some problems with cirrus clouds. However, the main drawback is that it is not able to estimate snow in pixels with less than 60% snow cover, and it does not work very well for snow in dense forests.

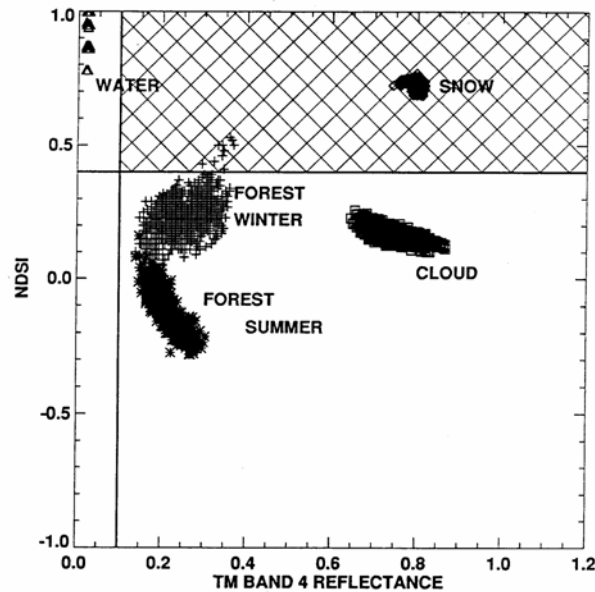


Figure 2.2. One version of a feature space for the SNOWMAP box-classification algorithm developed for MODIS imagery. It is here demonstrated with Landsat TM data. The crosshatched area is the class "snow" box. (Riggs 1995)

To improve the performance in forested areas, Klein et al. (1997) proposes to add a criterion comprising an additional area of the NDSI-NDVI space to be included in the class snow. This helps to include more of the winter-forested areas. He also proposed to consider the option of using band 7 instead of 6 in the NDSI.

2.2 Fractional snow cover retrieval

When frequent coverage is needed, a limited number of satellites are applicable. Examples of relevant optical sensors currently are AVHRR, MODIS, AATSR and MERIS. The spatial resolution is in the range 250-1000 m, which is actually quite coarse for many applications. In order to compensate for this, development of a sub-pixel or fractional snow cover area retrieval algorithm started already early in the era of remote sensing for hydrology applications in Norwegian. The idea dates back to a proposal in Østrem et al. (1979). The method is fully described in Andersen (1982). It is based on the assumption that there is a linear relationship between snow coverage and measured reflectance. When this relationship is established, it is an easy task to classify each pixel into snow cover percentage or a fractional snow cover categories. Four categories were used in Andersen (1982). The relationship is established by the use of

manual interpretation of a histogram of the image (as in the original approach) or by the use of calibration areas. A population of 100% snow covered pixels is identified and determines the reflectance for 100% snow coverage. A corresponding procedure is followed for 0% snow coverage. The method has been applied in Norway since it was developed, and has also been used in Canada (S. Ferner and I. Sutherland, 1987). It has later been refined and extended with automatic calibration, automatic geocoding and automatic cloud detection as described in Solberg and Andersen (1994). It is frequently referred to as the Norwegian Linear-Reflectance-to-snow cover (NLR) algorithm.

A relatively new approach to the problem of retrieving snow at the sub-pixel level is spectral unmixing. Spectral unmixing is particularly suited for sensors having a high number of bands, like imaging spectrometers, but it is also applicable to multi-spectral sensors like Landsat TM and ETM+. In spectral unmixing, it is assumed that a pixel is composed of several classes and the method tries to estimate the aerial coverage of each class. Hence, it does not rely on the assumption of one "background class" like NLR.

Nolin et al. (1993) introduced spectral unmixing for snow classification using a linear mixture model. It is assumed that there is a set of spectral endmembers ("clean spectral classes") that are combined linearly into the resulting pixel value. The task of classification is then to decompose the pixel into the correct contribution of each endmember (see Figure 2.3). Hopefully, an endmember corresponds to an actual ground cover class or subclass. The mixture model can be described as follows:

$$L_c = \sum_{i=1}^N F_i L_{i,c} + E_c$$

where L_c is the radiometrically calibrated radiance for band c , F_i is the fraction of endmember i , and L_c is the radiance of endmember i in band c . N is the number of endmembers and E_c is the error for band c to fit N spectral endmembers. The model results in a set of linear equations that

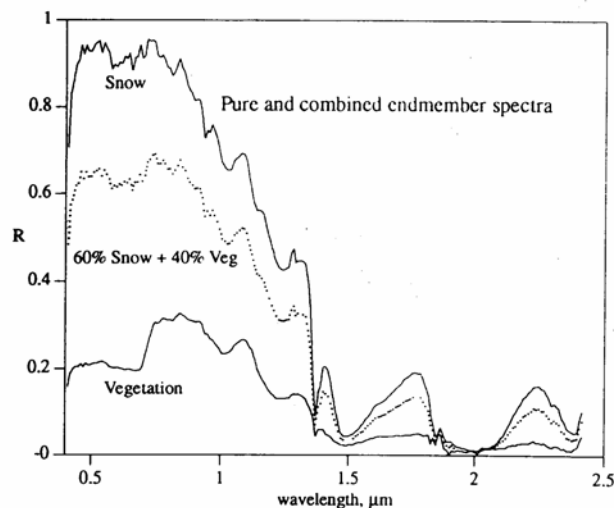


Figure 2.3. Reflectance spectra from AVIRIS showing snow, vegetation and a simulated spectrum of a linear mixture of 40% vegetation and 60% snow (Nolin 1995)

has to be solved. The approach is usually to minimize the error term E . Note that there may be several endmember mixture solutions which results in similar errors.

One advantage with this approach is that there is a measure of the fit between the model and the data, given by E . If the model does not fit the reality well, the error term may be large. A low error is an *indication* of an accurate result. The errors may be shown as the error image (error per pixel) or the RMS error for the whole image.

A disadvantage of spectral unmixing as applied in Nolin (1993) is that the method is supervised. The spectral endmembers have to be identified manually by training of the algorithm. Rosenthal (1996) proposes a method for unsupervised spectral unmixing. The method determines endmembers automatically and then compares them with spectra in a spectral library to estimate the mixture of each pixel. The method was tested on Landsat TM data and found to provide accuracy similar to what is obtainable from aerial photography for the test area.

A spectral library approach was investigated further in Painter et al. (1998). The main focus here was to take into account snow reflectance variability due to varying snow grain size. The grain size was mapped in the scene using an algorithm analysing a spectral absorption feature (Nolin, 1993). A library of snow spectra for varying grain size was then derived based on the grain size map. In addition, spectral endmembers for vegetation and rock was found in the image. These spectra and a shade endmember were used in an unconstrained linear spectral unmixing algorithm estimating the fraction of each endmember in a pixel by minimising the RMS error. The accuracy obtained for an AVIRIS image over a mountainous area was comparable to a snow map derived from an aerial image.

An automated approach following the basic ideas of Painter et al. (1998) was presented in Painter et al. (2003). A spectral library of snow, vegetation, rock and soil endmembers was used. The snow endmembers of varying grain size were derived from a radiative transfer model. The other spectra were measured in a laboratory and in the field. The same spectral unmixing approach was applied. An overall RMS error of 4% was obtained from analysing three AVIRIS images over a mountainous area and comparing them with aerial images.

The NDSI approach applied in NASA's SNOWMAP algorithm has recently been extended to retrieval of fractional snow cover (FSC). Salomonson and Apple (2004) tested whether there was enough "signal" in NDSI to map fractional snow. They selected a set of Landsat ETM+ images for various landscape types and classified those with the SNOWMAP algorithm. The binary classification result was aggregated up to 500-m pixels in the same grid as the MODIS 500-m product. An overall correlation coefficient of 0.9 and a RMS error of 0.1 were found for the linear regression result between FSC and NDSI. The algorithm has been validated and implemented for inclusion as a standard NASA MODIS FSC product, which was launched operationally in December 2006 (Salomonson and Appel, 2006).

An algorithm for retrieval of fractional snow cover based on an approach derived from remote sensing of aerosols over varying terrain has been tested by Kaufman et al. (2002). Snow has the same spectral property as aerosols of being dark at 2.1 μm . The pixel reflectance at 2.1 μm is used to estimate the reflectance of the snow-free area of the same pixel at 0.66 μm . The difference between the total pixel brightness at 0.66 μm and the estimated brightness of the

pixel for snow-free conditions is used to estimate the area fraction covered by snow, i.e. FSC. The method is expected to be most accurate for $FSC < 30\%$. The approach was tested for MODIS data covering a mountainous test site, giving highest accuracies for pixels of with low FSC, as expected.

Classification by neural networks has been used for many applications, including snow. Simpson and McIntire (2001) tested two types of neural networks to estimate fractional snow cover in NOAA AVHRR and NOAA GOES imagery. A feed-forward neural network was used to classify individual images, while a recurrent neural network was used to classify sequences of images. The continuous class variables were then post-processed into fractional land cover categories for mixed pixels. The results gave errors less than 10%. However, neural networks have a tendency to overfit the model to the given data set.

A method for mapping snow cover fraction at the basin level in forested areas has been proposed by Metsämäki et al. (2005). Reference images for full snow cover conditions are used to determine the reflectance reduction effect of the forest for each drainage basin. This relationship is then used to estimate the snow cover fraction for the basin under partial snow cover conditions. Comparison of a snow map for the entire Finland, based on NOAA AVHRR data, with in situ measurements (snow courses) gave an overall RMS error of 0.15.

If ancillary data about the forest type and distribution is available, such information could be used for more accurate retrieval of the snow cover in forest. Vikhamar and Solberg (2003a) present a method based on modelling of the reflectance from forested areas. The model takes into account the reflectance of the snow and trees, cast shadows on the snow and reduced diffuse irradiance due to hemispherical shielding caused by the trees. The snow-forest model was extended to non-flat (hilly) terrain in Vikhamar et al. (2004). The reflectance model represents the foundation of the fractional snow cover algorithm proposed in Vikhamar and Solberg (2003b). The algorithm makes use of a land-cover map to constrain linear spectral unmixing. The method was tested on a forested mountain area in Norway and gave overall error rates of less than 20% for 96% of the area.

2.3 Multi-sensor snow cover retrieval

Optical sensors are limited by cloud cover and current SAR sensors are limited to detection of wet snow. By combining optical and SAR sensors, it should be possible to monitor the snow cover more frequently. This is no new idea, but it was not practical to test out in large scale before frequent and large-scale coverage with SAR sensors was available in addition to optical data.

There are a few works on the combination of optical and SAR data published before large-scale SAR coverage become available. Raggam, Almer and Strobel (1994) demonstrated how snow cover retrieved from multi-parameter airborne SAR and SPOT HRV can be combined. Koskinen et al (1999) analysed a time series of NOAA AVHRR and ERS-2 SAR images. However, they did no actual combination of the two other than studying how the snow cover developed as observed by the two sensors. Tait et al. (2000) provides an example of a true combination of data from two sensors to produce a snow map. NOAA AVHRR data and SSM/I data are analysed together with climate station data and a digital terrain model in a decision tree in order to produce a continental-scale snow map for North America.

The situation of lack of access to frequent acquisitions of both SAR and optical data changed with the satellites Radarsat and Envisat (with ASAR) that in wide swath mode can deliver frequent coverage of a given geographical area. This allowed combination with AVHRR and MODIS on a frequent basis. Examples of such combinations can be found in Solberg et al. 2004a, 2004b.

Even more interesting is the combination of SAR and optical data on one platform that ensures acquisition under exactly the same snow cover conditions. The only platform delivering such data currently is Envisat. ASAR and MERIS can be acquired simultaneously. However, a significant drawback is that MERIS lacks thermal bands that can be used for cloud detection. Envisat has another sensor that allows cloud detection, AATSR. But AATSR has a much smaller swath width than ASAR and MERIS, so this gives no practical solution to the problem (anyway, an example of using AATSR for detecting clouds in a subsection of a MERIS scene can be found in Tampellini et al 2004). An example of the use of ASAR and MERIS in combination can be found in Solberg et al. 2004b.

3 NR's optical snow algorithms

The chapter present optical algorithms developed and improved by NR. Due to the relevance, also a multi-sensor time-series algorithm developed together with NORUT IT is presented.

3.1 The NLR snow algorithm

The optical snow cover algorithm is based on an empirical reflectance-to-snow-cover model originally proposed for NOAA AVHRR in Andersen (1982) and later refined in Solberg and Andersen (1994). The algorithm, also know as the Norwegian Linear Reflectance-to-snow-cover (NLR) algorithm, has recently been tailored to MODIS data by NR. It retrieves the Fractional Snow Cover (FSC) for each pixel. The model is calibrated by providing two points of a linear function relating observed reflectance (or radiance) to fractional snow cover (see Figure 3.1). The calibration is usually carried out automatically by using calibration areas. Statistics from the calibration areas is then used to compute the calibration points for the linear relationship.

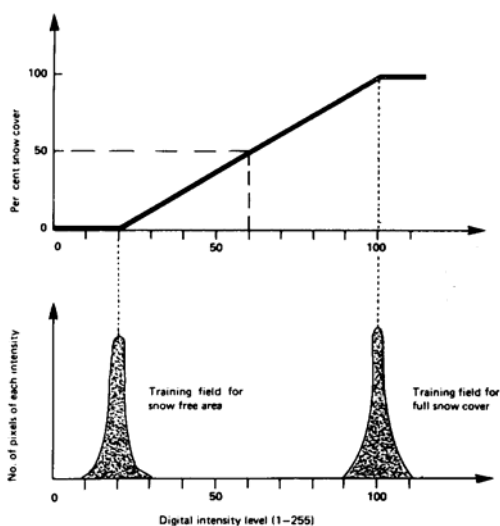


Figure 3.1. The Norwegian Linear Reflectance-to-snow-cover (NLR) algorithm illustrated. A pixel value is linearly transformed to a snow cover percentage. The algorithm is based on the assumption that the bare-ground reflectance is constant. (Andersen 1982)

A particular problem for practical use of the snow algorithm is clouds. NR has experimented with several approaches for cloud detection over snow-covered surfaces. The current best cloud detection algorithm is based on K Nearest Neighbour (KNN) classification of MODIS data. See more details in the next session.

3.1.1 The algorithm in detail

The main steps in the fractional snow cover retrieval algorithm are:

1. **Calibration of high-level spectral reflectance:** The upper parts of a fixed set of selected glaciers at high elevations are used as calibration targets for high-level spectral reflectance values. The average value and standard deviation is calculated for each calibration area. Calibration areas covered or partly covered with clouds are discarded (determined from the cloud mask). Calibration areas with high standard deviation or unusual average values are

also discarded (likely to include undetected clouds or fog; mean and standard deviation thresholds have been determined empirically and are fixed).

2. **Calibration of low-level spectral reflectance:** A fixed set of selected boreal forest areas with little human infrastructure and without agricultural fields are used as calibration targets for low-level spectral reflectance values. The average value and standard deviation is calculated for each calibration area. Calibration areas covered or partly covered with clouds are discarded (determined from the cloud mask). Calibration areas with high standard deviation or unusual average values are also discarded (likely to include snow or undetected clouds or fog; mean and standard deviation thresholds have been determined empirically and are fixed).
3. **Calibration of 100% FSC:** The spectral reflectance of 100% FSC is determined by a linear transformation of the average high-level calibration target values. The constants in the transformation have been determined empirically from a large set of images from several snowmelt seasons. Note that the constants are somewhat dependent on solar elevation (and therefore also the time of the satellite overpasses).
4. **Calibration of 0% FSC:** The spectral reflectance of 0% FSC is determined by a linear transformation of the average low-level calibration target values. The constants in the transformation have been determined empirically from a large set of images from several snowmelt seasons. Note that the constants are somewhat dependent of solar elevation (and therefore also the time of the satellite overpasses).
5. **Calculate FSC for each pixel:** The two calibration points calculated in Step 3 and 4 determine the linear transformation of at-satellite reflectance to FSC (as illustrated in Figure 3.1). For each pixel in the image not masked out by the cloud mask or the sea mask, FSC is calculated.

The algorithm above can be used in the visual and near infrared part of the electromagnetic spectrum. The blue area of the spectrum should be avoided as it is very sensitive to atmospheric haze. The near-infrared part of the spectrum may create problems late in the snowmelt season as the reflectance is significantly reduced as the snow grain size increases due to snow metamorphism. The green and red parts of the spectrums are “safest”.

The NLR algorithm can be regarded as a linear spectral unmixing algorithm using only one spectral channel. The algorithm unmixes the two spectral components representing snow and bare ground. The reflectances of the spectral components are determined by the calibration procedure. However, a weak point with this approach is that the spectral reflectance of all snow surfaces is regarded to be the same. The same assumption is made for bare ground. These assumptions are certainly not valid everywhere, but in practice the algorithm is working quite well anyway. This is probably due to the fact that some of the snow metamorphism is compensated for by the high-level reflectance calibration targets. Also, the algorithm is in principle only valid for unforested areas and has mainly been used in mountainous regions. The bare ground spectral variability in the mountainous areas is certainly far less than when also lower-elevation areas are included.

Another aspect is atmospheric correction. Such correction is not done explicitly, but some correction is inherent in the calibration procedure. As long as the atmosphere above the calibration areas is representative of the whole scene, atmospheric correction is included. To some degree the difference between lower and higher elevations is also accounted for. The high-level reflectance calibration areas are located at elevations of typically > 2000 m a.s.l., while the low-level reflectance calibration areas in the boreal forests are not significantly higher than at sea level. This means that as long as the FSC is correlated with the terrain elevation (FSC tends to increase with elevation), the effect of the variable optical thickness of the atmosphere is to some extent corrected for.

The algorithm does not include topographic correction. If not handled with care, topographic correction could make reflectance variability worse. When using a digital terrain model (DEM) to compute terrain correction, the geometric correction (geolocation) of the image must be very accurate in mountainous terrain. A positional error of 1 km (one AVHRR pixel), could easily result in a positional shift from a south-oriented slope to a north-oriented slope (or the opposite). Radiometric terrain correction using a DEM would when increase errors instead of reducing them.

FSC errors due to terrain orientation and slope can be found in snow maps based on the NLR algorithm. However, we have so far been conservative with respect to topographic correction in order not to increase errors. According to this, it is recommended to use images from times of the day when the sun is at its highest positions in the sky. For Norwegian latitudes, the algorithm is found to work reasonable well in the snowmelt season. However, one should be more careful when using the algorithm during the mid winter period.

As mentioned above, the algorithm is not aimed for forest-covered areas. In practice, it has to some degree been used in forested areas as well. When done with care, this usually works well. The presence of forest will reduce the reflectance as measured in the area covered by the pixel. This results in a reduction in the calculated FSC compared to the true FSC. However, the calculated FSC will always be higher than 0% when some snow is present. So, if one is only interpreting the FSC as a snow/no-snow flag (binary snow map), it works well. It would even be better to use a snow mask and threshold the calculated FSC-values into binary SCA values. If one wants a threshold representing 50% FSC rather than 0%, a threshold value could be determined empirically.

3.1.2 Processing flow

The processing flow for the generation of snow maps is shown in Figure 3.2. The process starts by downloading a new optical image data set from a data provider. This process is automatic and triggered by an email from the data provider (when the provider provides such a service). The data (image and metadata) are converted to an internal format. Then, cloud detection is performed followed by rectification of the MODIS image (geometrically transformed to a map projection) using the geocoding grid provided with the image product (for AVHRR an algorithm based on an orbital model is used, see Huseby, Halck and Solberg (2005)). Calibration area masks are used to identify the corresponding calibration targets in the image. Pixel value statistics is calculated for each area. The statistics are used to detect potential remaining clouds in the calibration areas or snow in the snow-free calibration areas, as described above. The accepted calibration areas are applied for determining the linear relationship between fractional snow and the pixel values. When the FSC retrieval process is completed, the result is

transformed to a raster product with metadata and stored in the type of format to be delivered to the user. Note that the whole process from image to snow map is completely automatic.

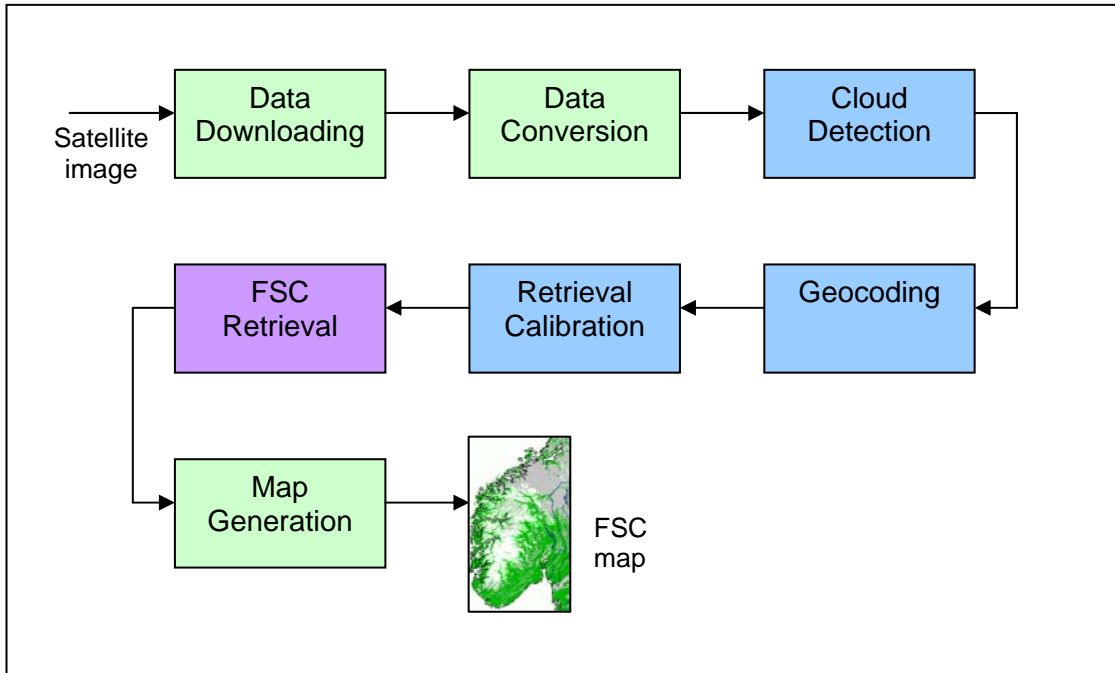


Figure 3.2. Processing flow for the generation of fractional snow cover maps from optical data based on the NLR algorithm



Figure 3.3. An example of a FSC map of South Norway. Clouds are shown in grey, ocean in blue and snow-free ground in dark green. FSC is shown in tones between white and green with white representing 100% FSC

3.2 Cloud detection in the presence of snow

A particular problem for practical use of the NLR algorithm is cloud detection. NR has experimented with several approaches, and the current best cloud detection algorithm is based on K Nearest Neighbour (KNN) classification of MODIS data. In a KNN classifier a pixel, represented by a vector of band values, is assigned the label, which is most prevalent among the K nearest labelled vectors from a reference set. A KNN classifier is an asymptotically optimum (Maximum Likelihood) classifier as the size of the reference set increases (Duda et al. 2001).

The classifier has been trained based on a set of partially cloudy images acquired through snowmelt seasons. For each image the bands 1, 4, 6, 19, 20, 26 and 31 are being used. Band 1 is available with a spatial resolution of 250 m, band 4 and 6 with 500 m and the other bands with a resolution of 1 km. Band 1, 4 and 6 are used in versions aggregated to 1 km resolution, and this is the resolution of the resulting sky detection mask. In addition, information about the sun angle is collected from the MODIS metadata file.

The seven bands applied cover wavelengths from 0.545 μm to 11.280 μm . The bands are chosen to get useful information for distinguishing clouds from snow, land and water. Band 1 and 4 are the red and green bands, which visually separates snow and clouds (together) from land and water. Band 6 contains information discriminating snow and clouds. For this band clouds have high, and snow low reflectance. Band 19 is sensitive to atmospheric water vapour. Band 20 and especially 31 contain information about the temperature of the land surface and the clouds. Band 26 is sensitive to water vapour and cirrus clouds. NASA uses 19 bands to make the MODIS cloud mask product (MOD35_L2), but using the seven bands mentioned seem to be more suitable for this regional application (note that the MODIS products are developed for global applications and had to be optimised for this purpose).

In order to obtain good performance of the KNN classifier, and since we have no prior information for weighting (as to which channels are the most important), we have chosen to use band variance normalization. A statistical analysis is performed over the training set, yielding means and variances of the image bands. The statistics is made for pixels where the sun elevation is higher than a certain specified angle.

A vector quantization codebook has been made for each training image, performing the following steps:

1. Correct for error pixels (found by statistical analysis)
2. Correct visual bands by scaling for sun angle
3. Compute standard deviation for each band
4. Normalize each band (scale to equal variance)
5. Cluster image vectors into specified number of clusters using a particular type of K-means named Myers Clustering (due to the initialization stage where extreme outliers are sought. This initialization method was first presented by Wayne L. Myers (Myers and Patil, 2006)
6. Rescale the cluster centres (removing the previous variance normalization)

We have used 1500 clusters. Each cluster is represented by a 7-dimensional vector.

A number of training images are then labelled manually. Each pixel should, if possible, be given a class label. In our initial reference set we use the following classes: cloud, land, ocean and snow. Reference vectors are extracted using a manually controlled spectral-distance based region-growing procedure. The procedure enables an accurate positioning of the spectral transition between different classes by utilizing the operator's ability to interpret both the pixel context and the pixel colour.

The pixel "colour" in this case is the RGB image obtained through a transform of each pixel vector. The colours RGB are assigned to the bands 1, 6 and 31, respectively (see Figure 3.4). This choice of colours shows ocean and land in blue, snow and ice in red/violet, and clouds in nuances of green/brown/beige. The clouds are in most cases easily separated visually from the other classes. A tool is developed to ease the manual labelling of images, a procedure which typically takes a couple of hours per image.

The labelled pixels change colour during the process, cloud – white, snow/ice – yellow, ocean – black, land – green, and multi labelled – red (see Figure 3.4). The operator selects a pixel with the cursor and selects a class. All pixels within the same cluster will then get the colour of this class. The operator can then select a region-growing threshold value. Then all pixels with cluster vectors spectrally close to the initial cluster vector will get the same colour. The operator can see if all these pixels seem to belong to the same class and label them, or one can extend or reduce the threshold value to extend or reduce the coloured regions before classification. Then the operator moves the cursor to another unclassified pixel and repeats the operations. Experience shows that one should not classify too large regions at the same time. Even if all pixels within the region close to your selected pixel obviously belong to the same class, there may be regions at other places in the image which are on the limit to other classes (mostly snow/ice). If you label these as cloud, you may later during classification of snow label the same

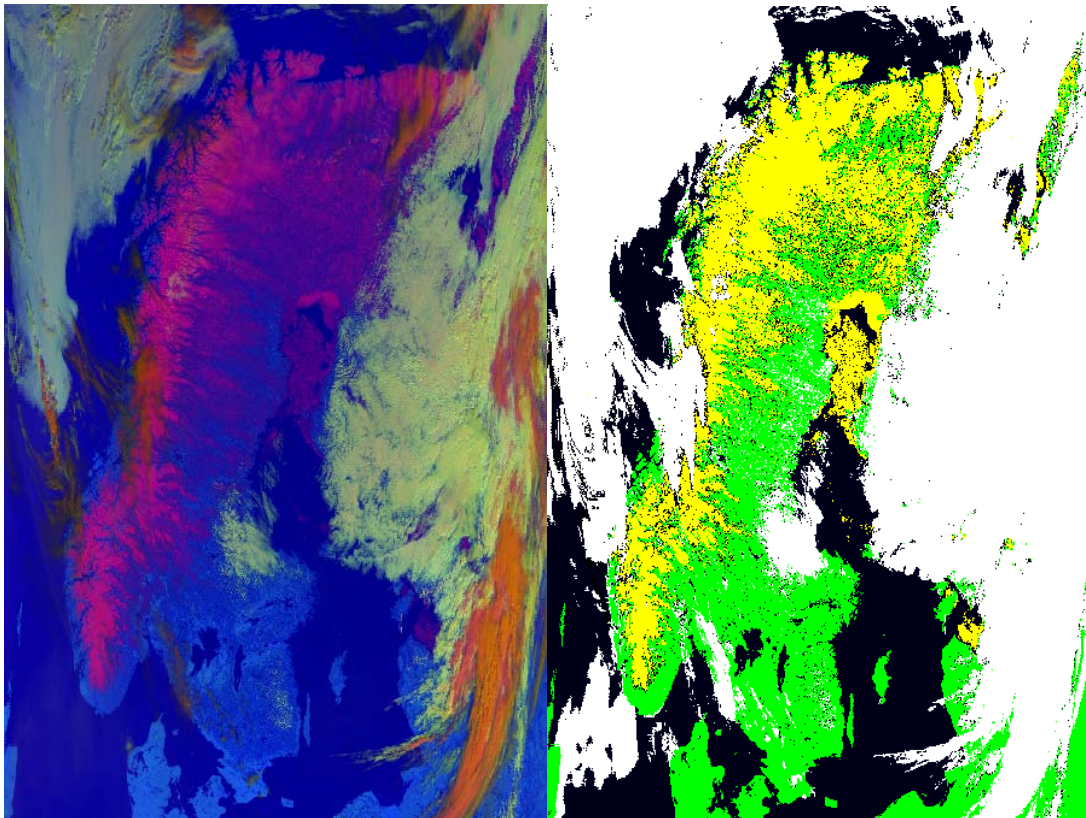


Figure 3.4. Intermediate steps in the cloud codebook development. Left: MODIS image before labelling. Right: Labelled image. The image is from 17 April 2003.

pixels as snow. The pixels will then be labelled to more than one class. These pixels will be marked with red, and the operator can later make corrections and relabel them. In the best case, all pixels should be labelled, but there will always be doubts, and the operator can leave pixels unlabelled. Unlabelled and multi-labelled pixels (cluster vectors) will not be included in the training set.

For each image a codebook is created, showing the relations between cluster vectors and classes. With a number of training images and 1500 cluster vectors per image the reference set is too large to carry out a cloud classification of a MODIS image in reasonable time. The final reference set size is reduced to a manageable size using standard vector-quantization (K-Means). A total of 500 representation vectors were used for each class.

3.3 NR's new optical snow model algorithm

In the approach for fractional snow cover retrieval presented here, the actual, current spectral BRDF characteristics of the snow and snow-free ground are modelled locally, per pixel. The models for full snow cover are established by assimilation of remote sensing data for varying acquisition and solar geometry during the snow and snow-free seasons. To model snow metamorphosis, a "time dimension" is introduced to let the spectral BRDF develop. The assimilation technique, using sensors with moderate spectral resolution, performs modulation of an initial spectrum of high spectral resolution to establish a full high-spectral-resolution BRDF model locally.

In order to be able to handle the development of the snow spectrum also when the snow cover is patchy, metamorphosis and impurity projection functions are introduced. These functions predict the development of the snow state during the late part of the snowmelt season. When the snow state is known, the current spectral BRDF can be determined using physical or empirical models.

With local estimates of spectra for snow and snow-free ground established, linear spectral unmixing is applied to estimate the current snow fraction per pixel. An iterative approach is used where the predicted spectra for snow and snow-free ground are improved in each iteration, hence also giving an improved estimate for the FSC.

The various parts of the method are described in more detail in the following sections. Preliminary results from the work behind the algorithm are also published in Solberg (2004 and 2005).

3.3.1 Spectral BRDF model grid

The snow undergoes a process of continuous metamorphosis and reception of impurities (the theory behind this is described in Wiscombe and Warren (1980) and Warren and Wiscombe (1980)). Snow crystals change structure and size, mostly due to processes related to energy transfer. Impurities, small particles of organic and inorganic material (like litter from vegetation, soil and soot), will usually be deposited in a rate proportional to the amount of vegetation and snow-free surfaces exposed to the air in the neighbourhood. Metamorphosis and increased impurity content change the reflectance spectrum. The near-infrared region of the spectrum is more sensitive to the metamorphosis than the visual part, while the visual spectrum is more sensitive to impurities.

The combined effect of terrain relief, solar illumination geometry and sensor acquisition geometry (here called geometrical effects) affects the exiting radiance for a given area on the ground (e.g., the area corresponding to a pixel). The atmosphere adds on with more effects for the observed radiance at the satellite.

Except for small experimental sites, it has proven quite hard to carry out fractional snow cover mapping through physical modelling of all or most effects mentioned. There are simply too many variables which one has no control over.

A fundamental aspect of the approach chosen here is to utilize observations as much as possible to retrieve the information needed that otherwise could have been created by complex, physical

modelling. In other words, empirical models have been used as far as it is possible when remote sensing can be applied to calibrate them.

An important part of the concept is that a spectral BRDF grid is established for the region to monitor. The grid size might correspond to the pixel size, such that there is one grid element for each observed pixel on the ground (however, this is no requirement and in general not true when different sensors are applied to monitor the same region). A grid element models the spectral BRDF for all relevant acquisition angles and solar illumination angles for the terrain relief associated with the given grid position.

Two BRDF grids are established – one for snow and one for the snow-free land surface cover (senescent vegetation, vegetation in the winter state when vegetation is present). The BRDF snow grid also has to model developing snow. Since the anisotropy of the snow reflectance changes with the metamorphosis and since the reflectance is depending on the local terrain orientation, there is no straightforward way to predict how the spectral BRDF for a snow grid element will develop with the metamorphosis. The approach taken here is to include a “time dimension” (or more correctly, a metamorphosis development dimension) to the spectral BRDF model. The metamorphosis dimension in the grid model is parameterized by the observed or effective grain size (various algorithms for retrieval of the effective grain size are presented in Fily et al. (1997)).

The grid is calibrated using a spectral BRDF assimilation algorithm. The BRDF grid elements are built up from numerous observations, through several snow seasons, to reach full coverage of combinations of snow metamorphosis and illumination and observation geometry. Similar assimilation is done for snow-free surface conditions during late spring and autumn (with senescent vegetation). It is important to avoid any presence of bare ground in the snow grid and any presence of snow in the land surface grid. This is done by a comparison of each new observation with statistics for the corresponding grid element. If the new observation represents a spectral BRDF outlier, it is discarded. For initialization of the grid, to build up the initial statistics, special filters are applied to ensure pure observations.

index and snow grain size index values are low. For snow-free ground (early-spring) conditions, it is checked that the pixels have low chlorophyll content and no snow present.

3.3.3 Metamorphosis and impurity projection

For fractional snow cover conditions, snow metamorphosis and the level of impurities cannot be directly measured due to the spectral mixture of snow-free ground and snow. The terminal full snow cover conditions are here used as a baseline for projection algorithms. There is one model for nominal development of metamorphosis and several models for nominal development of the impurity concentration.

The metamorphosis model builds on a degree-day approach to simulate the metamorphosis (similar approach is often taken in snowmelt models). Since the temperature normally will not be available, nominal development for the given region is applied. The local BRDF spectrum from the relatively stable winter conditions is applied as a reference spectrum. This spectrum includes the effect of the terrain and tall vegetation. The developing spectrum is modelled by a BRDF model (see previous section).

The process of impurity deposition in the snow is mostly driven by the wind for areas with low vegetation, and most of the deposition takes place when snow-free ground appears in the neighbourhood. The deposition process has been measured in the field for the development of fractional snow cover for several land-cover types. The measurements are the basis for empirical functions parameterized by snow cover fraction. There is one function for each general land cover type.

The BRDF model and the impurity model each provide a new snow spectrum. The spectra are fused into an estimate of the current snow's BRDF spectrum with estimated impurity content.

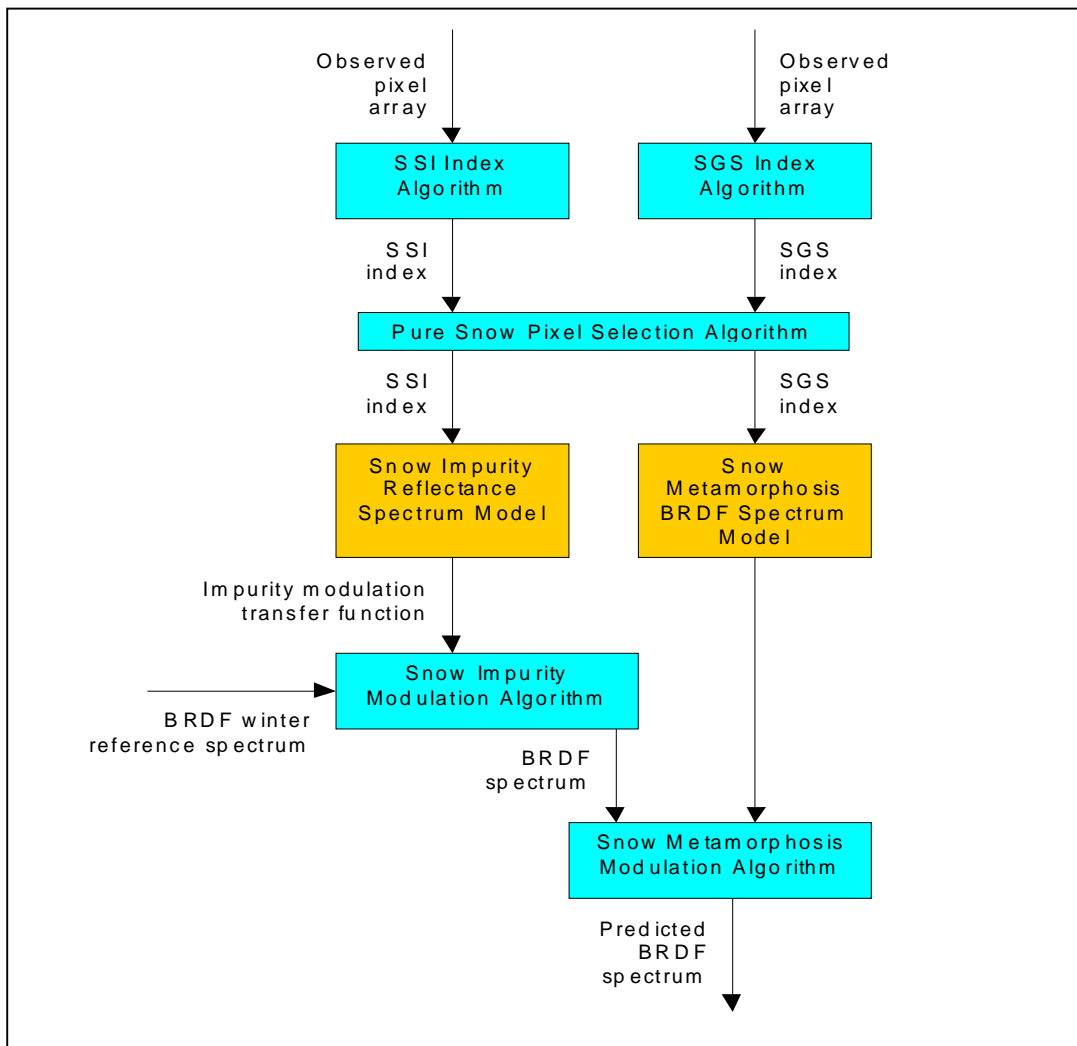


Figure 3.6. Conceptual design of the method for snow-development BRDF spectrum prediction

3.3.4 Fractional snow cover algorithm

For the fractional snow cover algorithm, it is assumed that snow and bare ground BRDF databases have been built up by the assimilation algorithm. The snow development model is then applied for predicting new spectra based on current observations of the grain size and the contents of impurities. For fractional snow cover conditions, bare ground is detected by an abrupt increase in the snow impurity index. The snow development model will then fail, so projection models are applied during this phase of the snow season. Predicted spectra are input to a conditional spectral unmixing algorithm. By using “most likely spectra”, a more reliable result would be obtained as linear spectral unmixing in general gives many solutions (the true solution cannot easily be selected without additional information).

The overall approach for the fractional snow cover algorithm is illustrated in Figure 3.7. The algorithm starts to calculate an initial estimate for the snow cover fraction. A simple two-spectra linear mixture model is applied, where the two spectra represent the terminal full snow coverage as determined by the snow spectral BRDF grid and the snow-free surface as determined by the snow-free surface spectral BRDF grid.

The algorithm proceeds with metamorphosis modelling, parameterized by the estimate of the snow cover fraction. The terminal full-snow-coverage snow spectrum is modulated accordingly.

The next step is to model impurity deposition. A map of local land cover type is used to select the relevant model, and snow cover fraction is used to parameterize the model. The estimated impurity content is used to further modulate the snow spectrum.

The next step is to apply the modulated snow spectrum, i.e. the predicted snow spectrum, and the corresponding grid element for the snow-free surface in a linear spectral unmixing algorithm. This gives a new and more accurate estimate for the snow cover area fraction of the current pixel.

The algorithm proceeds in an iterative manner applying the new estimate of the snow cover fraction to make a new, and hopefully better, estimate of the snow spectrum, which is again applied in the linear spectral unmixing algorithm. The process is repeated until the change between two iterations is marginal or an upper limit for the number of iterations is reached.

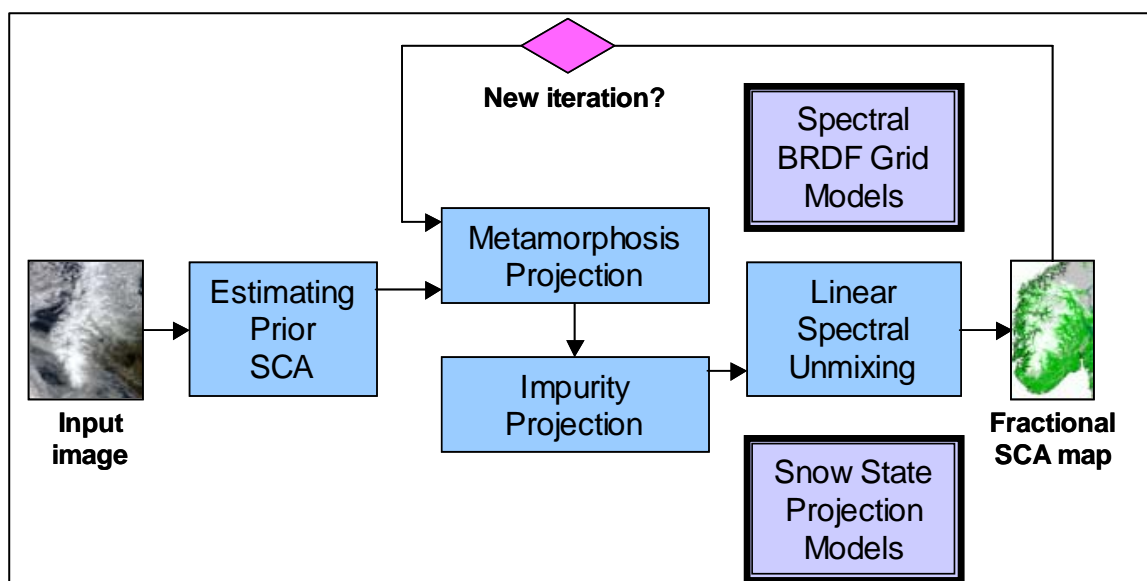


Figure 3.7. Overall approach for the new fractional SCA algorithm

3.4 Multi-sensor time-series snow cover algorithm

The overall idea behind the algorithm is to combine optical and SAR sensors and utilise the best features of each sensor when possible in order to map snow cover area (SCA) more frequently and with better spatial coverage than would otherwise be possible. Optical remote sensing algorithms are able to map snow cover quite accurately, but are limited by clouds. SAR sensors penetrate the clouds, but current algorithms for satellite-borne sensors are only able to map wet snow accurately.

The sensor fusion approach developed takes place at the level of geophysical parameters. A few algorithms for multi-sensor time-series processing have actually been developed. One approach is to analyse each image individually and combine them into a day product. How each image contributes to the day product is controlled by a pixel-by-pixel confidence value that is computed for each image analysed. The confidence algorithm is able to take into account, e.g., information about observation geometry, probability of clouds, prior information about snow state and reliability of the classification. The time series of day products are then combined into a multi-sensor multi-temporal product. The combination of products is done on a pixel-by-pixel basis and controlled by each individual pixel's confidence and a decay function of time for the product. The "multi-product" should then represent the most likely status of the monitored variable.

The algorithm development also includes a near-real-time product where a new snow map is produced for each satellite image received. The two approaches, day product and near real time, were developed by NR and NORUT, respectively. Only the day product is described here (see NORUT publications for more on the near-real-time product).

More information about the fusion approach can be found in Solberg et al. (2004a, 2004b and 2005).

3.4.1 Baseline algorithm

The basic idea behind the algorithm is to apply daily optical data and supply with SAR data as frequently as practically possible. SAR data have to be limited to the melting season due to the fact that current satellite sensors are only able to retrieve wet snow. Furthermore, current cost regimes for optical and SAR data might in practice limit the use of SAR data, while optical data are much cheaper. From practical experience so far, approximately 1-3 SAR image acquisitions per week is adequate.

The overall multi-sensor time-series algorithm can be written as follows:

$$MSCA_i(x,y) = USCA_i(x,y) \quad (1)$$

for i which gives $\max(\text{conf}_{time}(i) \text{ conf}_{MSCA}(USCA_i(x,y))) \quad i = t, \dots, t-n$

where $MSCA$ is the new multi-sensor time-series SCA product, $USCA$ is a "time-unit" product (a single-sensor product or a day product), $\text{conf}_{time}(t)$ is a time-dependent confidence function, conf_{MSCA} is the confidence function for the "time-unit" product, t is the current day and n is the number of days in the time series. In other words, for each pixel (x,y) select the "best" time unit i from a time series of unit products. "Best" means the pixel with maximum confidence. Hence, the selection process is entirely controlled by the confidence function.

The confidence function $conf_{time}(i)$ is a decay function of time, i.e., a function giving reduced confidence as the age increases of each unit product (see Figure 3.8). The function might be linear giving largest confidence to today's observations and no confidence above a given time horizon.

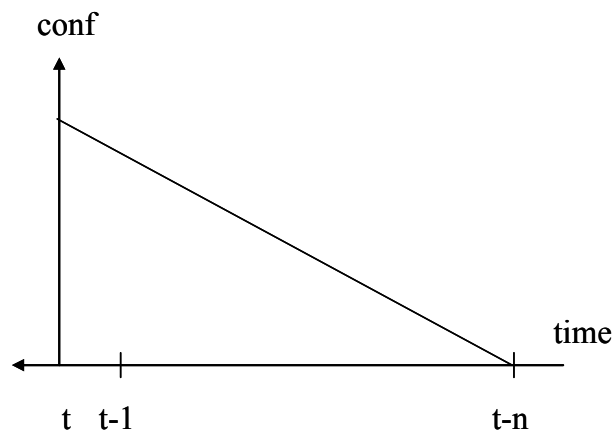


Figure 3.8. Linear confidence function decreasing the confidence of a time unit product by $1/n$ per time unit

Single-sensor products as well as day products have associated per-pixel confidence values. The confidence values for a day product are the combination of confidence values in the respective single-sensor products where pixel values have been selected. The optical single-sensor product applied in the algorithm has so far been based on the NLR algorithm, however, with an extension including the computation of per-pixel confidence values. Products from the new snow model algorithm may be applied in the future. The SAR single-sensor product is based on NORUT's SAR algorithm (Storvold et al., 2006; Nagler and Rott, 2000).

A single-sensor confidence function is typically related to acquisition geometry, trust in the decision taken by the retrieval algorithm, etc. The following single-sensor confidence functions have been found to be relevant:

Optical pixel confidence: $conf_{SCA-OPT} = c_s() c_c() c_d()$

- c_s : Confidence function related to pixel sample ground size (increases with distance to nadir)
- c_c : Confidence function related to cloud probability (clouds may be transparent)
- c_d : Confidence function related to snow age (snow grain size and impurities increases with time and reduces contrast)

SAR pixel confidence: $conf_{SCA-SAR} = c_{cl}() c_g() c_t()$

- c_{cl} : Confidence function related to classification confidence (distance to threshold)
- c_g : Confidence function related to acquisition geometry (snow contrast depends on incidence angle)
- c_t : Confidence function related to air temperature in reference and new image (from met. stations)

The confidence values are in range between 0 and 100. Zero confidence means that no SCA value has been estimated. This refers to water, forest and radar shadowed areas in the SAR products, and to classified clouds and large view angles ($> 60^\circ$) in the optical products.

For the sensors and retrieval algorithms applied in the experiments in this report, the optical products yields a fractional snow cover for each 250 m pixel, while the radar products yields the snow cover as a classification into snow/no-snow for each 100 m pixel. The radar product is resampled to 250 m, thus resulting in a quasi-fractional snow cover product for SAR.

3.4.2 Day-product approach

This version of the algorithm uses day products as the time-unit products. The multi-sensor time-series algorithm takes the form:

$$MSCA_t(x,y) = DSCA_i(x,y) \quad (2)$$

for i which gives $\max(\text{conf}_{\text{time}}(i) \text{ conf}_{DSCA}(DSCA_i(x,y)) \quad i = t, \dots, t-n$

A day product is defined as a merge of single-image products as follows (pixel indexing has been skipped for clarity):

```

for (each product  $SSCA_i$  of this day)                                     (3)
  if ( $\text{conf}_{DSCA}(SSCA_i) > \text{conf}_{DSCA}(DSCA)$ )
    then  $DSCA = SSCA_i$ 
  else if ( $SSCA_i = \text{CLOUD}$  and  $DSCA = \text{UNCLASS}$ )
    then  $DSCA = \text{CLOUD}$ 

```

Here, $SSCA$ is a single-image product and $DSCA$ is the day product (initialized with "UNCLASS"). In other words, if there is one or more cloud-free optical or radar observations for a given pixel position that day, select the single-image product pixel with highest confidence. Otherwise, the pixel is set to "CLOUD". The approach assumes that there in general are multiple acquisitions each day, either optical or a mixture of optical and SAR. It is also assumed that the SCA in practice will not change during the day, which means that multiple observations during a day represent observations of the same snow-cover situation.

The term "CLOUD" refers to pixels that have been observed, but where the observation has been discarded, i.e. the confidence is zero. For optical images, the term "CLOUD" is meant literary, but for day-products including ASAR observations, the "CLOUD" class refers to pixels where all observations are non-confident.

The day-confidence function, conf_{DSCA} , is the product of the single-sensor confidence function (for either optical or SAR) multiplied by an inter-sensor confidence factor, $\text{conf}_{\text{INTER-OPT}}$ and $\text{conf}_{\text{INTER-SAR}}$. This factor makes it possible to give one sensor different confidence scaling than the other.

4 Evaluation of NR's optical snow algorithms

This chapter provides an evaluation of the algorithms described in Chapter 3. The algorithms have been evaluated in different contexts (e.g., projects) and there is no rigorous inter-comparison of them available. The NLR algorithm and the cloud algorithm are also compared with NASA's standard MODIS products as a reference.

4.1 The NLR algorithm

In the study behind this section, NLR FSC products based on MODIS data have been compared with various reference images of better resolution. Candidates for "ground truth" were Landsat images and aerial photographs. Landsat images have a resolution of about 30 m and from aerial photographs we have orthophotos of 1 m resolution.

The NLR production chain with NR is currently producing FSC maps of both 250 m and 1 km resolution. In EuroClim, the products have pixel size of 1×1 km, while other projects have used products of pixel size of 250×250 m. We have used the algorithm on MODIS images of 250 m resolution in the validation work presented here.

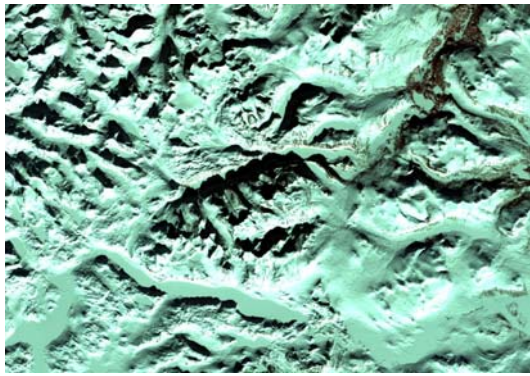
To be able to compare the results from various times in the melting season, we had to define a validation area, which was covered by all the images in the study. We chose an area of 2280 km² (57×40 km) in the eastern part of Jotunheimen in South Norway. This area includes the Valdresflya-Heimdalen test site where many field campaigns have been carried out and which is covered by several orthophoto mosaics. As the SCA algorithm is developed for use in terrain without forests, the chosen area contains very little forest. In the eastern and southern part of the area there is a mixture of flat areas and terrain without abrupt changes, but in other parts there are high and steep mountains, which complicates the snow cover classification.

4.1.1 Data set

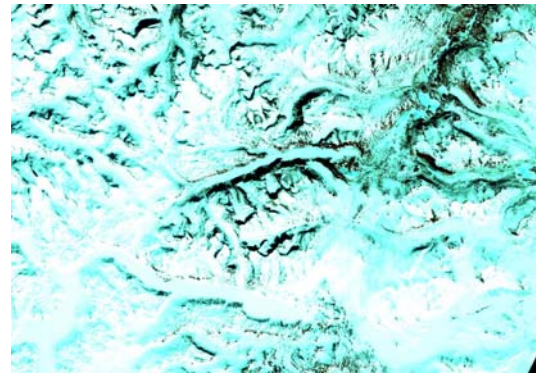
MODIS images from a number of dates in the winter and melting season were compared with Landsat images and orthophotos from the same days. The number of days for comparison was limited by the existence of useful Landsat images covering the validation area.

Table 4.1. Landsat images used in the validation

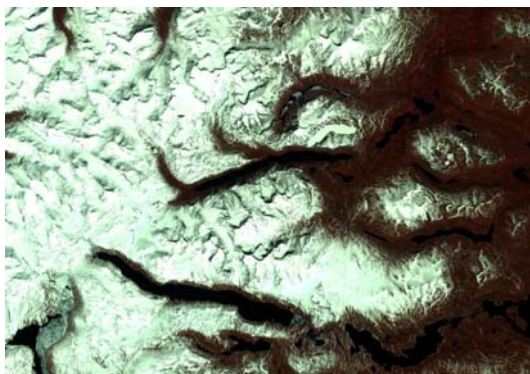
Date	Satellite	Sensor	Path	Row
2003.03.01	Landsat 7	ETM+	200	17
2003.04.18	Landsat 7	ETM+	200	17
2004.05.23	Landsat 5	TM	199	17
2004.05.30	Landsat 5	TM	200	17
2003.08.09	Landsat 5	TM	199	17



2003.03.01



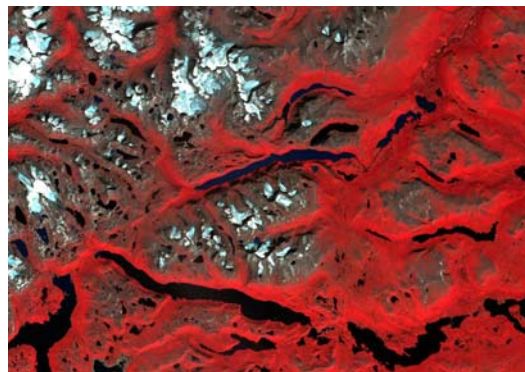
2003.04.18



2004.05.23



2004.05.30



2003.08.09

Figure 4.1 Landsat images used in the validation. Only the validation area is shown.

For 2003 and 2004 we found five Landsat images without clouds obscuring the validation area. They are from early March until early August, representing time periods with nearly 100% snow cover through decreasing snow cover until as close to a minimum you can get. In 2003 there was extremely little snow, and in the beginning of August there was practically no snow left outside the glaciers.

Figure 4.1 shows subsets of the Landsat images of the validation area. The colouring is a result of using band 4, 3 and 2 as RGB. The images give a good view of the change of snow conditions during snowmelt seasons.

A list of the MODIS images used in this study can be found in Table 4.2. The given time is the start time (GMT) of the acquisition. For two of the days we have studied two images taken at different times to see the influence of the acquisition time on the SCA product.

Table 4.2. MODIS images used in the validation

Date	Time
2003.03.01	1100
2003.04.18	1100
2004.05.23	1005
2004.05.23	1140
2004.05.30	1010
2003.08.09	1000
2003.08.09	1140

For 2004 we had aerial photographs taken 13 June, covering the Valdresflya-Heimdalen test site, which is included in the validation area. An orthophoto with a resolution of 1 m was made from these photographs, see Figure 4.2.

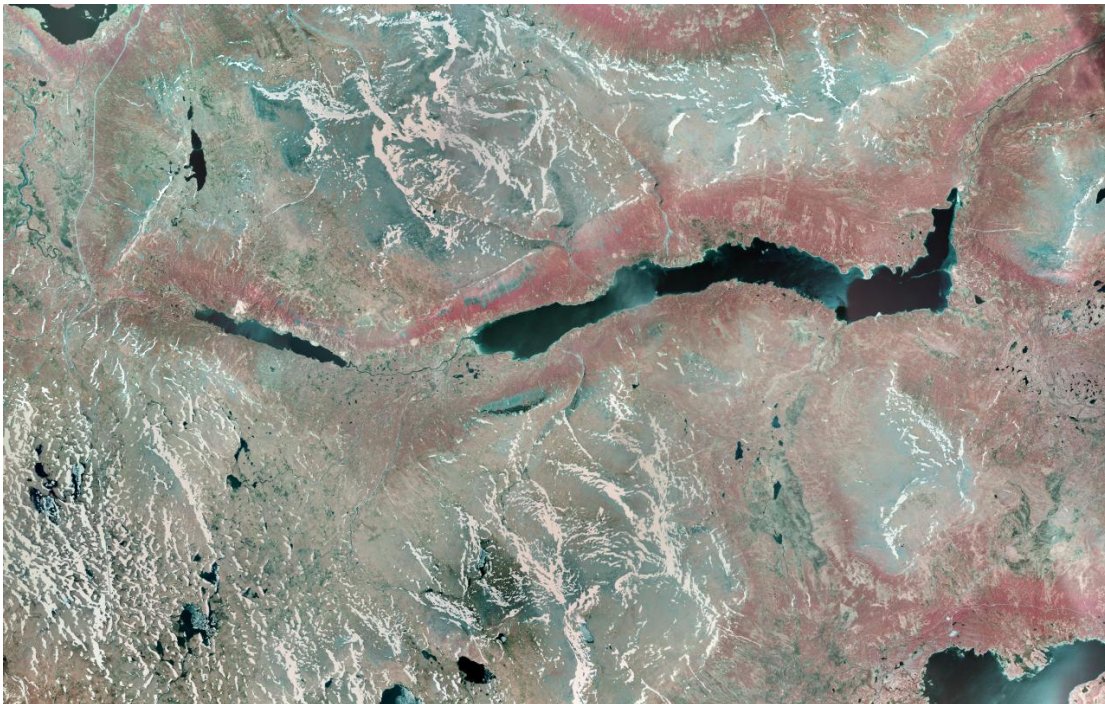


Figure 4.2. Orthophoto of Heimdalen test site. The photos were acquired 2004.06.13

Snow cover area was estimated for all the MODIS and Landsat images. To be able to compare the results, the images were geo-corrected to the same projection. Due to the projection of existing calibration data and the use of the data in other projects, the images were corrected to UTM zone 33 north in WGS84.

The Landsat images were corrected using a special Landsat correction function in ERDAS Imagine. A detailed vector water mask was used to select control points and a digital elevation model was also used as input for the correction procedure. The images were resampled to pixel size 25×25 m to make it easy to compare with MODIS images of resolution of 250×250 m.

4.1.2 Snow classification

The snow classification was performed by unsupervised ISO clustering in ENVI. The processing was limited to the validation area. For all images the clustering started with 10 clusters. It showed up that the results differed substantially. For some of the images it was necessary to introduce more clusters to be able to extract the snow classes. And in some cases a better result was obtained by only using one or two bands. See example in Figure 4.3.

In all cases the results showed one or more classes representing 100% snow and one or more clearly to represent bare ground. In addition there were one or more classes, which in some parts of the image seemed to be snow or partly snow, but in other parts looked like snow-free areas. Some of the pixels are only partly covered with snow and the reflectance is lower than for pixels completely covered with snow. Older snow changes colour because of particles blown in from the snow-free surroundings and the reflectance decreases. Therefore, a pixel completely covered with old snow may look as if it is partly covered with new snow. Snow in a slope facing towards the sun reflects more light than in slope facing away from the sun. Therefore, a pixel completely covered with snow, facing towards north, may look like a pixel only partly covered with snow. The result is that in all images there is an uncertainty about the total snow area. The found clusters are combined into three classes (see example in Figure 4.4):

1. Complete snow cover
2. Partly snow cover
3. Bare ground

We operate with three numbers, a *minimum* snow cover, which includes only the pixels classified to 100% snow (Class 1), a *maximum* cover, where 100% snow cover is also assumed in the pixels with uncertain classification (Class 2), and a *mean* cover, where it is assumed that the snow cover is 50% in the uncertain pixels. The minimum is definitely a too low estimate, far too low for some of the images. The maximum is probably too high. We then have lower and upper limits for the total snow cover and a number for a probable snow cover area.

From visual inspection, the selected Landsat images had no clouds within the validation area. Accordingly, we did not have the problem of separating snow and clouds. For most of the images, there were serious problems of classification due to shadows. This occurred especially for the images from March and April when the sun is rather low and the shadows are long. But because of the high and steep mountains, the problem was present in some places even May and August. To be able to detect snow in the shadows, we tried to extract more information from these areas. The square root function in ENVI was applied on the images before classification. This improved the snow classification substantially.

To be able to compare the classified MODIS images directly with the results from Landsat classification, the Landsat images had to be resampled to 250 m resolution. This was done by making one 250 m pixel out of one hundred 25 m Landsat pixels. The snow cover percent in this pixel is being calculated by counting the number of Landsat pixels with complete snow cover

and adding the number of pixels with 'partly' snow cover, adjusted to 50% snow cover (see examples in Figure 4.4).

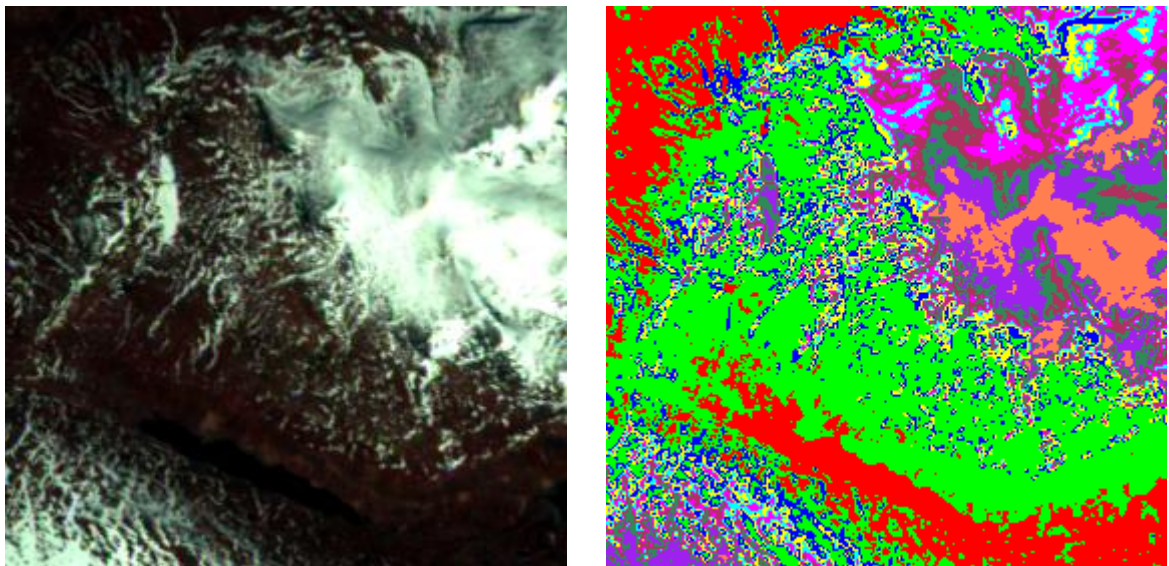


Figure 4.3 Left: Part of Landsat image from 2004.05.23. Right: The image after unsupervised clustering into 10 classes.

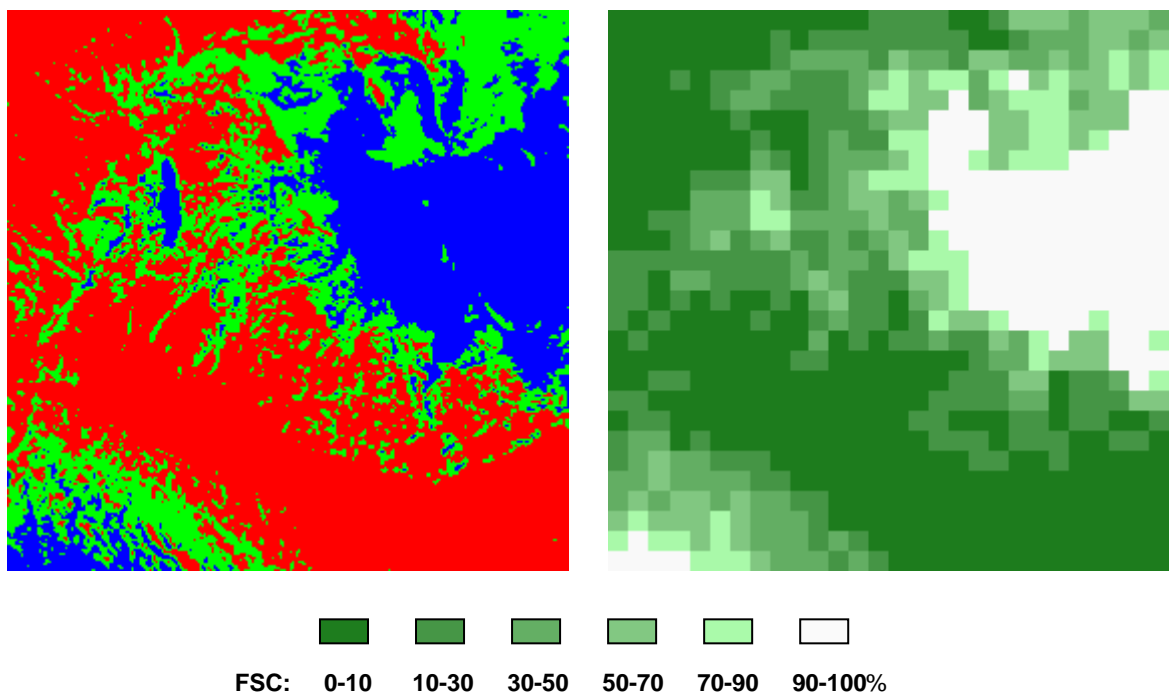


Figure 4.4. SCA classification from supervised clustering of the image in Figure 4.3. Left: Blue - 100% snow cover, green - partly snow cover, red - bare ground. Resolution 25 m. Right: Snow cover percentage, resolution 250 m

The MODIS images were processed in the NR production chain. The geo-correction is performed by an algorithm developed at NR, using geolocation information given in the MODIS image files.

The snow classification algorithm uses calibration areas located at various places in southern Norway, and the classification was performed for whole South Norway. From the classified images, the results from the validation area were extracted.

The classified image shows the snow cover area given in percent per pixel. To find the total snow cover area, one has to add all pixels with snow taking the snow fraction into account.

In the classification process, the program has to detect clouds in the image. NR has developed a cloud classification algorithm for MODIS data of 1 km resolution. To be able to compare the classification results with the Landsat images, one has to detect the clouds in both types of images. To make it easy, we have chosen Landsat images showing no clouds in the validation area. However, the cloud classification program detects clouds in the validation area in all the MODIS images. This means that the cloud classification algorithm is far from perfect. The Landsat and MODIS images are taken so close in time that it is very improbable that such an amount of clouds should appear or disappear so quickly.

A problem with cloud detection seems to occur along the borders between snow and bare ground. For 2003.03.01, when the area is totally covered with snow, just a few extra clouds have been detected. However, later in the melting season, this effect may cause serious errors in the estimated total snow cover area. This happens because snow classification has not been performed in the areas covered by the detected clouds. To solve this problem in the validation, we have removed the clouds in the cloud mask for the validation area.

The snow classification algorithm is made for open areas without forests. The classification results in forested areas will not be reliable. To avoid this problem we applied a forest mask and compare the snow cover for areas without forest only. The forest mask with 250 m resolution is created from a mask with 30 m resolution.

The snow classification of the orthophoto was done in the same way as for the Landsat images using ISO clustering. The results were not satisfying. There are variations in the pixel intensity in the orthophoto which make the snow areas look quite different in various parts of the photo. These differences cannot be seen in the paper version of the orthophoto. There are also areas of sand and gravel which look quite different from the snow in the paper versions, but which look similar to snow in the orthophoto. The result is that there are large areas of snow which are not classified as snow, and areas with sand and gravel which are classified as snow. Then we have no good estimate of the amount of snow from the orthophoto, and cannot use it to validate the FSC product.

4.1.3 Results

The classified Landsat images with SFC in 250 m resolution are shown in Figure 4.5. The calculated total snow cover outside forests in the validation area can be found in Table 4.3. The classified MODIS images are shown in Figure 4.6. Full snow cover is shown in white and partial snow cover in nuances of green from light to darker towards dark green for bare ground. The forest mask is shown in black.

Taking a look at the classified MODIS image from 2004.05.23 at 11:40 in Figure 4.7, one can see that there is classified snow between the forest and the lake at the southern bank of Gjende. This should not be possible, since the forest is growing down to the lake and the snow limit is high

above the forest according to the Landsat image. The explanation must be that the correction of the MODIS image to the selected projection is not perfect. A study of the corrected images with water vector data overlay shows that the accuracy of geolocation varies from image to image. The offset seems to vary between 0 and about 500 m, with a mean value of one pixel (250 m) or less. This means that one will not get exact results if one tries to compare images pixel by pixel to see the difference in classification.

The offset was checked only inside the validation area. Further investigations need to be done to find the offset in a complete scene and see if it varies over the scene. From Figure 4.7 one can see that the 250 m forest mask is not completely correct compared to the vector land mask. This is due to the transformation of the mask from 30 m to 250 m resolution. A small offset in some places will have very little influence on the calculated FSC.

The classified MODIS and Landsat images can be compared in many ways. One way is to compare the images pixel by pixel to see the difference in classification. This will not give useful result in all cases. The MODIS snow maps show the percentage of snow cover for each pixel. The classified Landsat images, resampled to 250 m resolution, show the same, but the percentage is calculated by counting the 25 m pixels classified as completely covered with snow within the resampled 250 m pixel, and adding the pixels classified as partly snow covered, adjusted to 50% snow cover. Comparing the MODIS and Landsat images in this way, you can detect locations where there are serious differences, but to give exact quantitative differences are of less value.

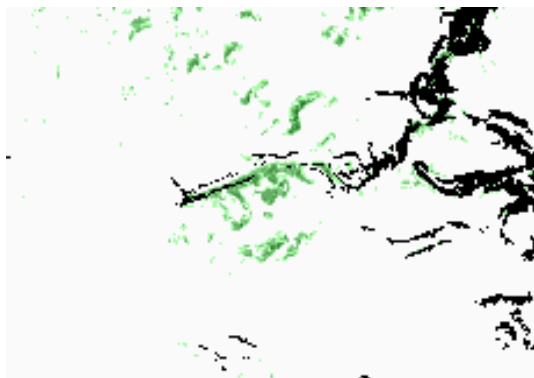
As the geocorrection of the MODIS images is not perfect, one will not always be able to compare pixels covering the same geographic area, thereby creating differences even if there are no differences in the snow classification.

Difference images have been calculated by subtracting the classified Landsat images, resampled to 250 m resolution, from the corresponding MODIS SCA images. From these images it is possible to detect where the NLR algorithm gives false results. In Figure 4.8 the difference between MODIS and Landsat classified images is shown for three days where there are small errors in the geocorrection of the MODIS images. In the white areas, there are no difference between the FSC value calculated from MODIS and Landsat. Colours from yellow via orange and red to dark red show where the MODIS FSC image shows too little snow. Cyan through light blue, blue and dark blue show where the MODIS snow map has higher FSC values than those calculated from the Landsat image.

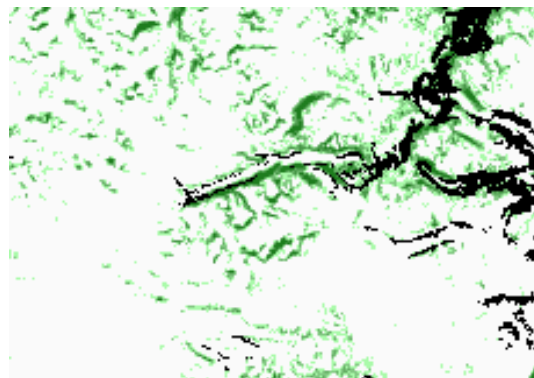
From Figure 4.8 some main trends can be seen. For 2003.04.18 with a nearly complete snow cover, the snow cover is correctly (white) or close to correctly (yellow) estimated in horizontal areas and slopes facing towards south. On the large lakes the algorithm finds less than 100% snow cover for some reason (some open water?). In the slopes facing towards north there is a large underestimation of snow cover (shown in red).

For 2004.05.30 the ice has melted on the lakes. Except for a couple of glaciers the snow cover is largely underestimated in areas with a certain amount of snow (orange and red). The effect of slopes facing toward north is reduced. On the borders between snow and bare ground, the MODIS algorithm finds more snow than the estimates from the Landsat image (cyan). There are only small differences, which may be due to the way the snow cover percentage is calculated

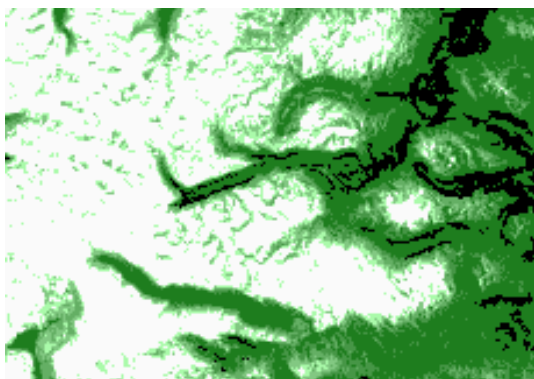
for the Landsat images. In some places the blue colour shows an estimate of more snow for MODIS. This is partly due to a small offset in geo-location between the two images.



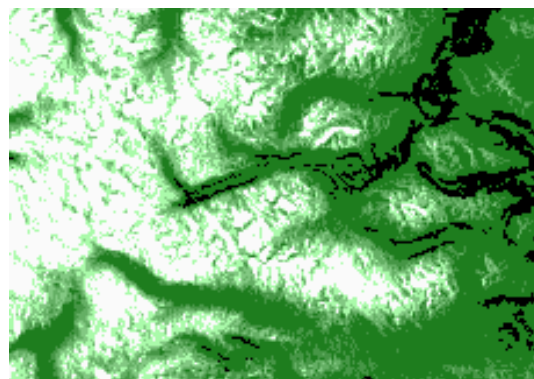
2003.03.01



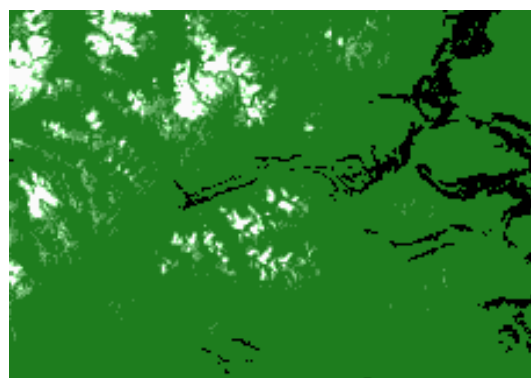
2003.04.18



2004.05.23



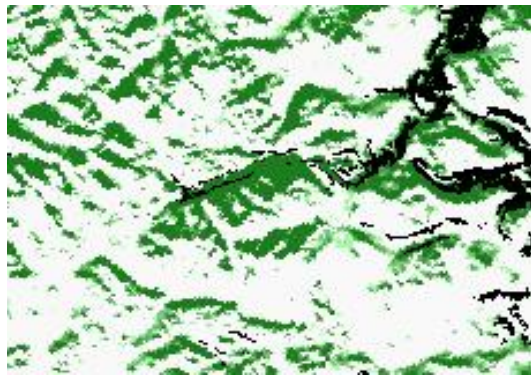
2004.05.30



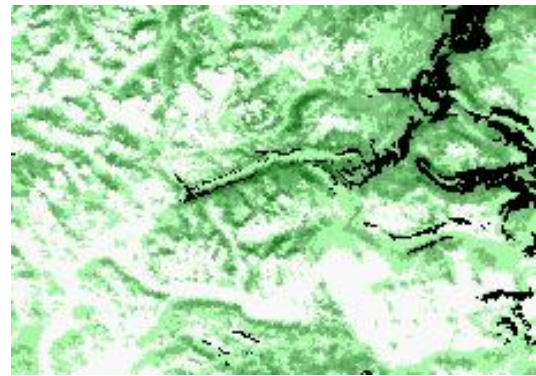
2003.08.09

Figure 4.5. Classified Landsat images resampled to 250 m resolution. Use of colours is explained in Figure 4.4

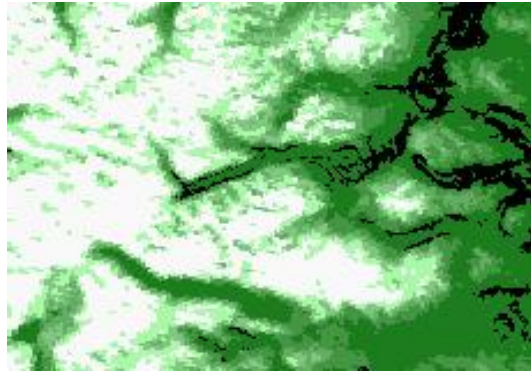
For 2003.08.09 we see a severe underestimation of the snow cover (dark red). Also here we see overestimates in areas with very little snow. In addition the MODIS algorithm finds snow in areas where there clearly is no snow.



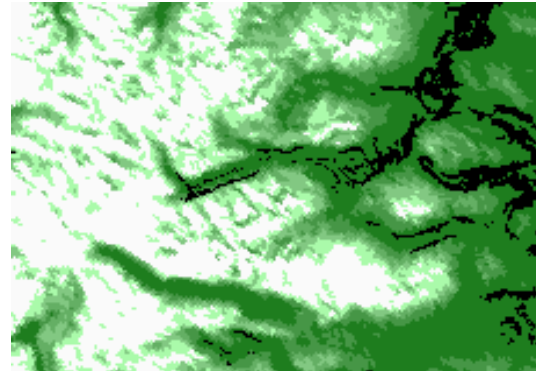
2003.03.01 11:00



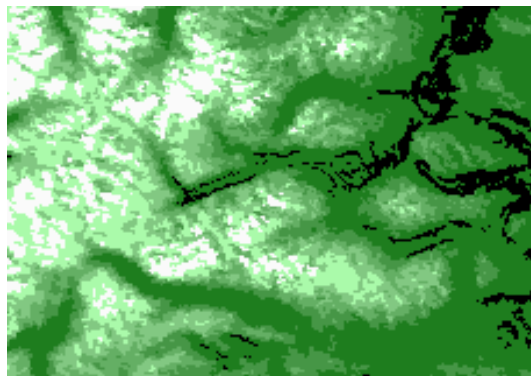
2003.04.18 11:00



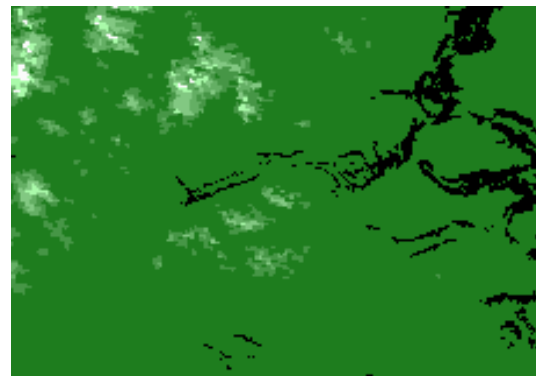
2004.05.23 10:05



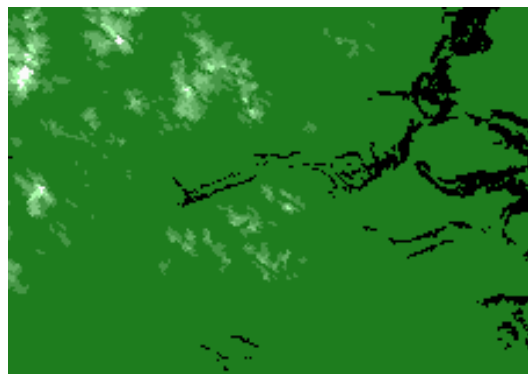
2004.05.23 11:40



2004.05.30 10:10



2003.08.09 10:00



2003.08.09 11:40

Figure 4.6. SCA classified MODIS images. Use of colours is explained in Figure 4.4. Forested areas in black.

A simple way to validate the snow cover classification is to calculate the total snow cover area in the validation area for both types of images and compare. Because the MODIS images are not perfectly geo-corrected, the validation area will vary somewhat in location, but not so much that it should influence seriously on the total snow cover area.

The total validation area is 2280 km². The calculated size of the forest area is 129.125 km² on MODIS images, using mask with 250 m pixels, and 129.0775 km² on Landsat images, using 25 m pixels. Therefore, the area for snow calculations will differ slightly: 2150.875 km² for MODIS and 2150.9225 for Landsat.

In Table 4.3 the calculated SCA is given in km² and percentage of the total non-forested area for corresponding MODIS and Landsat images.

Table 4.3. Calculated SCA for MODIS and Landsat images

MODIS			Landsat SCA		
Date and time	SCA		Min	Mean	Max
2003.03.01 – 11:00	1575.493	km ²	2096.479	2116.450	2136.421
	73.25	%	97.47	98.40	99.33
2003.04.18 – 11:00	1650.198	km ²	1929.821	1988.572	2047.323
	76.72	%	85.51	92.47	99.42
2004.05.23 – 10:05	1227.877	km ²	1132.568	1321.705	1510.841
	57.09	%	52.65	61.45	70.24
2004.05.23 – 11:40	1167.005	km ²	1132.568	1321.705	1510.841
	54.26	%	52.65	61.45	70.24
2004.05.30 – 10:10	845.749	km ²	805.359	1042.862	1280.365
	39.32	%	37.44	48.48	59.53
2003.08.09 – 10:00	83.044	km ²	113.414	161.318	209.223
	3.86	%	5.27	7.50	9.82
2003.08.09 – 11:40	74.124	km ²	113.414	161.318	209.223
	3.45	%	5.27	7.50	9.82

In Table 4.4 the estimated SCA from the MODIS images is shown in percent of the mean value found in the corresponding Landsat images, and the difference in calculated snow cover area.

Table 4.4. SCA estimated from MODIS relative to mean value of Landsat estimation, and difference in area.

Date and time	SCA MODIS relative to Landsat in %	SCA difference km ²
2003.03.01 – 11:00	74.44	540.957
2003.04.18 – 11:00	82.98	338.374
2004.05.23 – 10:05	92.90	186.400
2004.05.23 – 11:40	88.30	247.272
2004.05.30 – 10:10	81.10	197.113
2003.08.09 – 10:00	51.48	78.274
2003.08.09 - 1140	45.95	87.194

From Table 4.3 one can see that there is a large uncertainty in the SCA estimated from the Landsat images. It varies from image to image with minimum variation for 2003.03.01 (97.47–99.33%) and maximum for 2004.05.23 (45.98–70.24%) and 2004.05.30 (37.44–59.43). The main reason for the difference in uncertainty lies in the snow distribution. In the image from

2003.03.01 the area is totally covered with snow. There are just some very steep hillsides without snow. The problem with shadows has been solved, so most of the snow in the shaded areas has been detected. In the other images the snow has started melting, and there are large and small patches of snow, which complicates the classification. We have the problem of pixels partly covered with snow, and old snow with lower reflectance. For 2004.05.30 the snow fragmentation was extensive, so the number of pixels with uncertain amount of snow was very large. For 2004.05.23 the classification resulted in some classes where large areas were completely covered with snow and small areas in the same class obviously partly covered. Assuming 50% coverage for these classes probably gives a too small value for the calculated mean SCA value.

Table 4.3 shows that the NLR algorithm used on the MODIS images underestimates the amount of snow in all cases. Except for 2004.05.23 and 2004.05.30 the derived SCA is even below the minimum Landsat values for all images.

In Table 4.4 the estimated SCA from MODIS is compared with the calculated mean Landsat value. Remember that this is not an exact value of the snow cover area, but an estimate with an amount of uncertainty, which is hard to specify. We see that the estimated SCA varies from 45.95% to 92.90% of the estimated 'correct' value.

The value of 92.90% is probably far too high. The estimated mean SCA value of 2004.05.23 from the Landsat image is very uncertain. As we do not know the correct value, we cannot say for sure that the result from 2004.05.23 is better than 2003.04.18 or 2005.05.30.

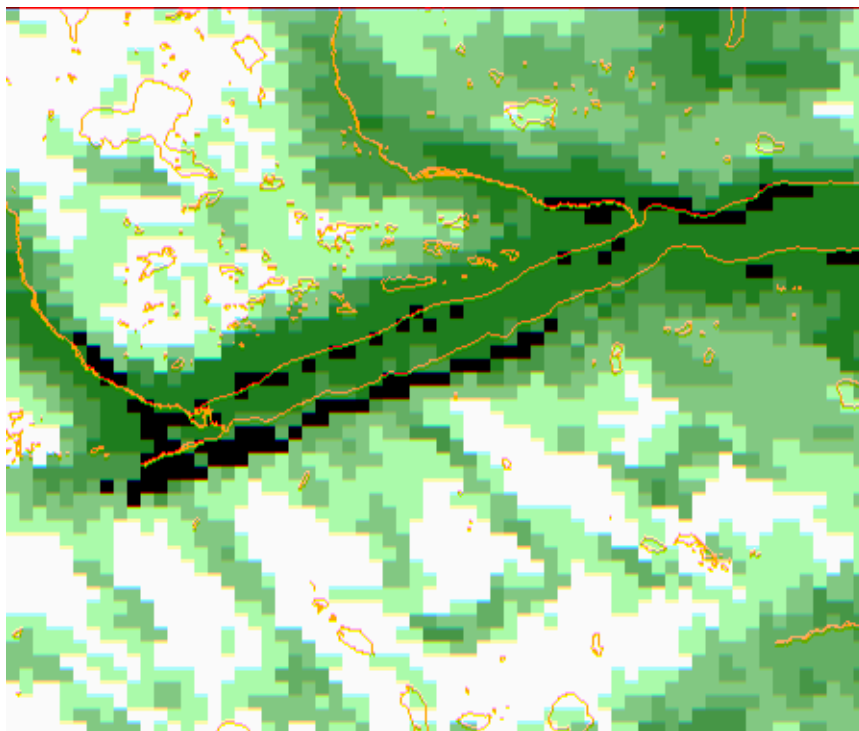


Figure 4.7. Part of the classified MODIS image from 2004.05.23 near lake Gjende, with overlay of vector data for water and forest

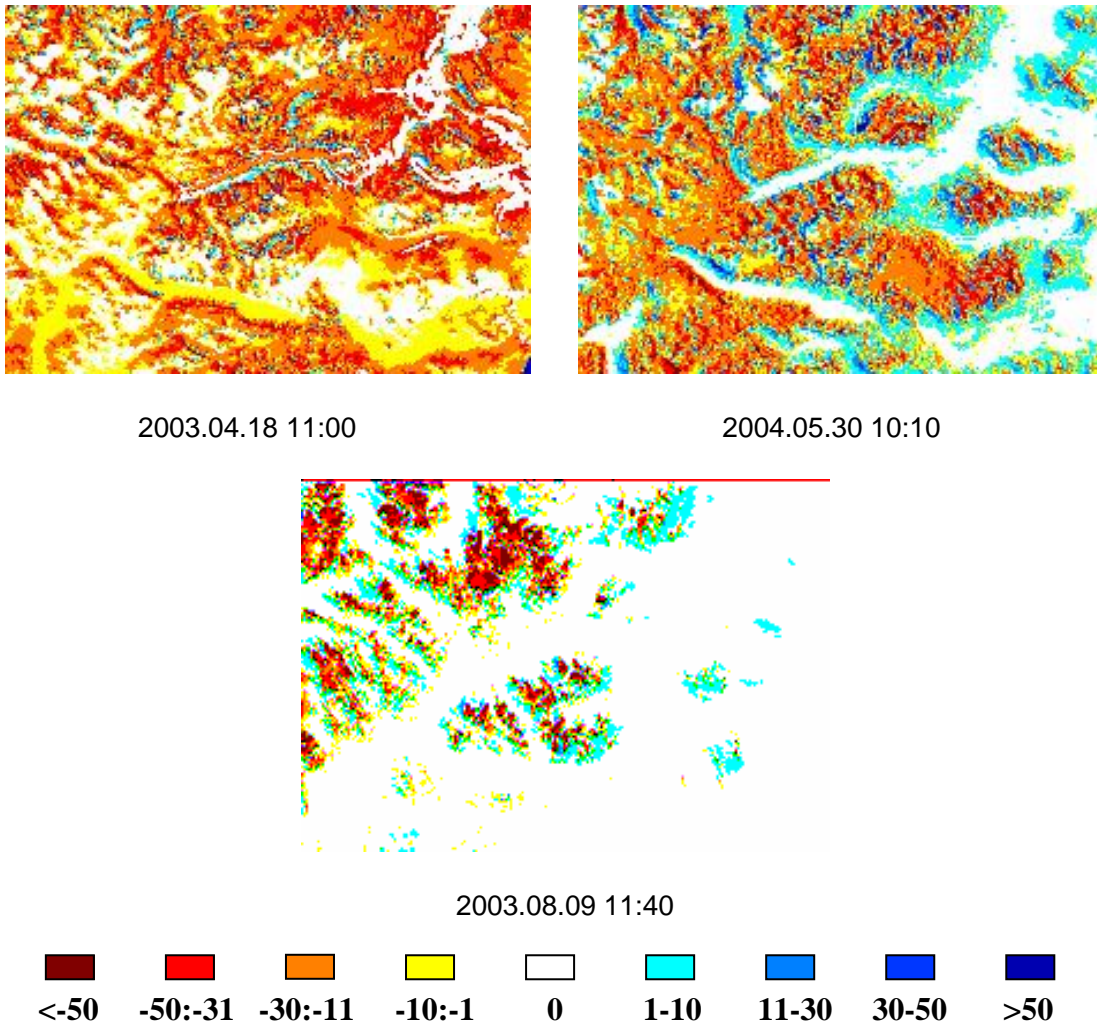


Figure 4.8. Difference images. The colours show the difference between calculated SCA for MODIS and Landsat in percent

Some specific comments to the results from looking at Figures 4.5, 4.6 and 4.8 in combination with Table 4.3 and Table 4.4:

2003.03.01: The low sun makes large shadows all over the area, and is the main reason for the low SCA estimate. The effect of slopes away from the sun adds to the miscalculation. The low sun makes most slopes towards north lie in shadow and the calculated SCA is mostly 0 or 100%.

2003.04.18: The sun is higher and the shadow effect is reduced. Still the slopes away from the sun have an important effect. There has been little melting and there is probably not much pollution influence. The calculated result is good.

2003.05.23: The shadow effect is minimal, and the slope effect is reduced. The melting has been going on for a while, and there is probably some polluted snow. For this day we have two MODIS images with quite different values of calculated SCA. The difference is 60.9 km². The difference could be explained by different sun height and

different aspect angle from the satellite. The middle of the validation area lies at 9° east, which give the maximum sun height at 12:24 local time or 11:24 GMT. The images are from 10:05 and 11:40 GMT. The last image has the best sun height. The view angle from the satellite is between 45.94° and 49.03° degrees for the 10:05 image and between 41.53° and 45.15° for the 11:40 image. The best view conditions should then be for the 11:40 image. However, the best SCA result was derived from the 10:05 image. It is difficult to tell why. One reason could be the direction of the slopes relatively to the position of the satellite. At 10:05 the validation area is seen from east and at 11:40 from west. If there are larger areas of steep hills towards east than west, the view from east might detect more snow. In Jotunheimen there are more steep hills facing north and east than south and west. If one compares the two images from this day, one will see more areas with low SCA values in the 11:40 image along mountain ridges. This could explain why there was more snow detected in the 10:05 image, but this needs a closer study.

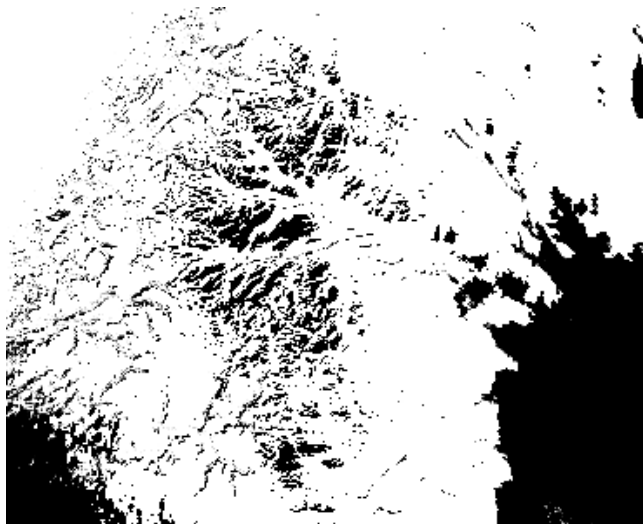
2004.05.30: There has been extensive melting during the week from 05.23. The snow is more fragmented and more polluted. One could expect a worse result than the week before. From Figure 4.8 one can see that the underestimation also occurs in horizontal and slopes facing toward south. The rather large differences from the Landsat estimates could partly be due to a too high snow cover percentage in the Landsat calculations. A small overestimate in areas with very little snow can be explained by the uncertainty in the way the snow cover percentage is being calculated in the Landsat-based estimation.

2003.08.09: Usually one should expect the result of SCA calculation to be worse during the summer due to more polluted snow and appearance of old snow and ice. The extremely bad result of SCA calculation can be explained by the special condition this summer. Almost all snow from the last winter was melted, even on the glaciers. This is very unusual. As for 2004.05.23 the best result was obtained from the image acquired in the morning.

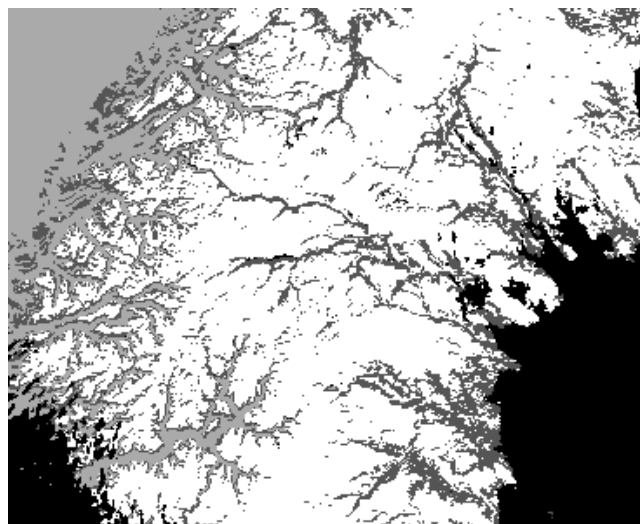
Figure 4.8 shows very large differences between the estimates in the areas classified as 100% snow cover in the Landsat images. This is expected because the snow is dark. In some areas without snow the NLR algorithm finds snow. This can be explained by the extremely large snowmelt this summer. In areas, which are covered with snow most time of the year, rocks have a much lighter colour than rocks at lower elevations due to lack of lichen cover. In such areas, the NLR algorithm could result in $FSC > 0\%$.

4.2 The cloud detection algorithm

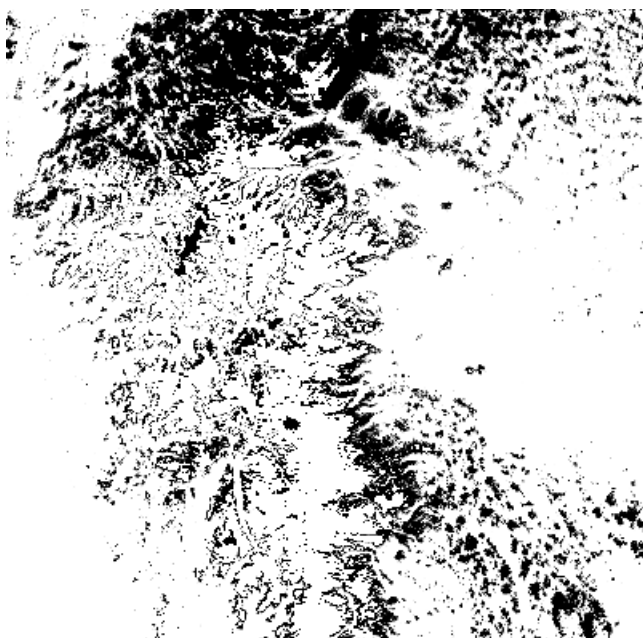
Tests have shown that for most images including snow, our KNN-classifier based method produces a better cloud mask than the mask available from the MOD35_L2 MODIS product provided by NASA. A couple of examples will show the difference. We show a part of a MOD35 mask (clouds in black) and our corresponding mask covering parts of southern Norway. Our mask shows clouds in black, and in addition the other classes used in the KNN-classification are shown (snow in white, land and water in gray).



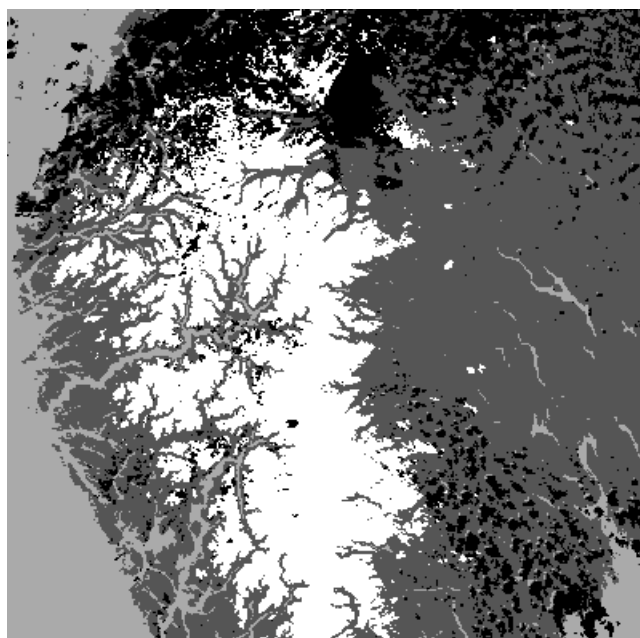
MOD35 1 March 2003



Cloud mask 1 March 2003



MOD35 17 May 2002



Cloud mask 17 May 2002

Figure 4.9. A comparison between the cloud mask from NR's cloud detection algorithm and the MODIS MOD35 cloud product

Large systems of clouds and smaller cloud systems over bare land are detected quite similarly by both methods. There are small differences, which one sees when studying the examples, but the main difference lies in detection of clouds over and at the borders of snow-covered areas.

In cases with cold weather and dry snow, the MOD35 algorithm will sometimes show clouds over snow covered areas when there are no clouds. In the example from 1 March 2003 in Figure 4.9 this is clearly seen. Visual inspection of the MODIS input image and a Landsat image shows that there are no clouds in the mountainous areas, and yet the MOD35 mask shows clouds over the highest areas.

In the example from 17 May 2002 in Figure 4.9 another typical error in MOD35 masks is shown. Visual inspection comparing a MODIS input image and a Landsat image acquired about simultaneously shows that outside the larger systems of clouds in the north and south-east, there are some minor cloud systems near the fjords, but in the snow covered areas there are practically no clouds.

This is reflected in our cloud mask, but MOD35 shows clouds along most of the edges of the snow covered area, and also over the snow in some distance from the snow edge in the eastern part of the southern snow areas. In the image from 1 March 2003 this border effect is not significant. Estimates of the snow surface temperature shows that the snow is cold and dry in all the mountainous areas. For 17 May 2002 the estimates shows that the snow temperature is close to 0 almost everywhere, except in the regions with the highest elevations where it is colder. In these regions our cloud mask also shows some clouds, but not as much as the MOD35 mask. It is obvious that the temperature of snow and clouds will influence on the cloud detection. To improve the detection, one should probably have different codebooks for winter, spring and summer.

4.3 NR's new optical snow model algorithm

The focus of the validation work has so far been on BRDF and impurity models, the most critical components of the approach, and the accuracy of the resulting FSC retrieval results.

Validation of the BRDF model is almost impossible to do by in situ measurements for inhomogeneous areas, like mountainous terrain, as the satellite sensor and ground instruments measure reflectance on very different scales making it hard to relate the measurements to each other. The approach selected here is by means of airborne profiling for inhomogeneous areas and also by field measurements for winter snow when larger areas are homogeneous.

4.3.1 Validation approach

A field spectrometer has been adapted for airborne measurements and connected with a digital still-image camera. The spectrometer and the camera observe the same field of view. An almost continuous spectral function is made by the spectrometer. The spectral resolution can be resampled to the same as for the BRDF model. The flying altitude sets the spatial resolution. The camera and the spectrometer log the time of the samples continuously. The timing makes it possible to relate the two sources to each other afterwards and to actually see the surface area leading to the measured spectrum. Varying angles are obtained by changing the across-track viewing angle using a pan-tilt platform. Geographical relation to the satellite observations is done by means of aircraft attitude control, and GPS logging making it possible to accurately position the profiling track on the ground. BRDF validation is then straightforward by comparing profiling reflectance values with those generated by the BRDF model. The image recording is used as a control of the co-registration of the satellite and aircraft measurements and for providing additional information in order to be able to understand the spectral measurements (often needed in steep terrain where small variations of the position gives large variations in the observed spectral signature).

For FSC, comparison is done with high-resolution measurements from satellites and aircrafts that provide the "true" SCA. Landsat TM and ETM+ images have been classified using a semi-automated approach, as described in the previous section. Clustering has been applied initially to segment the image according to the natural spectral classes at hand in the given image. This has been followed by manual merging of classes in order to produce a snow/no-snow map. A similar approach has been followed for aerial imagery resulting in snow maps of 1 m pixel resolution. Digital still images acquired with the spectrometer/camera platform described above, have also been analysed this way.

4.3.2 First experimental results

The new method for FSC retrieval is just in the first stage of validation. Therefore, only results from the first few and limited experiments are presented here. The quantitative results should be interpreted cautiously as larger experiments for a broader variety of snow conditions need to be carried out to understand how the algorithm performs in general.

The first experiments have been carried out in the Heimdalen-Valdresflya test site in the Jotunheimen mountain region in the central part of southern Norway (9.0° E; 61.4° N). The area is of about 200 km² with an elevation range of 1050 to 1840 m a.s.l. The area is free of tall vegetation except for some birch in the lowest locations.

The experiments so far have concentrated on the snowmelt season in 2004, for the period April-June. The site is usually fully snow covered in most of April, and snow patches may remain until late June. Fractional snow cover area has been retrieved from Terra MODIS data and compared to Landsat 5 Thematic Mapper (TM) images and one aerial orthophoto mosaic. The available TM images were acquired 23 May and 30 May, while the aerial photos were acquired 13 June. The TM images have been classified interactively using a clustering algorithm. The 30 m classified pixels were then converted to 250 m pixels of fractional snow cover for direct comparison with the maps derived from MODIS data with the new algorithm. The orthophoto mosaic with 1 m spatial resolution is quite hard to classify due to radiometric effects from the varying viewing geometry within each original image, so the mosaic has so far been used for comparison of small areas only.

The snow maps have also been compared to maps generated by the NLR algorithm. The NLR algorithm has previously been compared to the NASA GSFC MODIS algorithm in Hall et al. (2004), where the algorithms were shown to give quite consistent results.

The snow cover was quite patchy on 13 June. Field measurements also showed that there was a significant amount of impurities in the snow. The NLR algorithm gave too low values in the area, typically 25-20% less SCA than the orthophoto shows. The new algorithm gave values typically within 5% of the orthophoto.

The comparison with snow maps derived from the TM images included studies of mountain slopes in various directions (see Figure 4.10). The NLR algorithm might in many cases give snow fractions up to 30-40% higher than the actual value for slopes oriented towards the sun and, similarly, 30-40% lower values for slopes oriented away from the sun. The new algorithm, which indirectly compensates for the terrain orientation relative to the sun, gave values within approximately 5% of the values derived from TM.

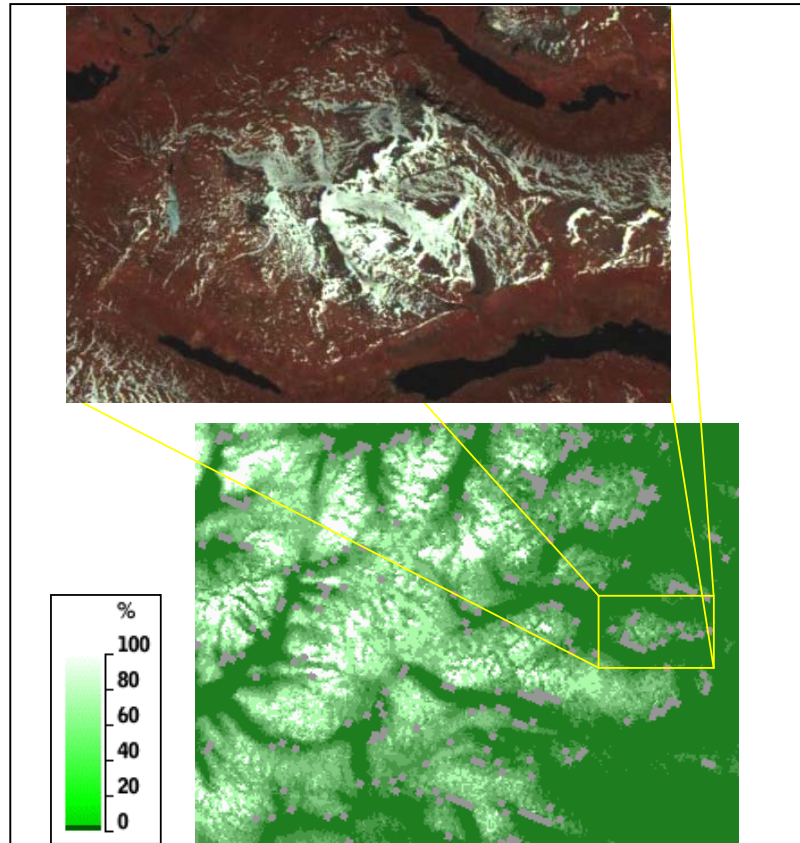


Figure 4.10. Landsat TM image acquired 30 May 2004 showing Heimdalsshø mountain in the Heimdalen-Valdresfylla test site. The NLR algorithm gave much too low values in the northerly oriented slopes, up to 40% too low SCA was found in this example. The new method gave errors within about 5% for the same slopes

4.4 The multi-sensor time-series snow cover algorithm

The experiments described in the following have been carried out partly for a test site where several field campaigns have taken place as well as acquisitions of aerial images for snow reference map generation. Additionally, experiments were carried out for South Norway in general where Landsat TM and ETM+ images have been used for reference when available.

The test site Heimdalen-Valdresflya has been applied for aerial imaging and field campaigns. Hourly temperature observations were available from the nearby stations at Bygdin (1050 m a.s.l.) and Bitihorn (1607 m a.s.l.). The time series of image data is from the period 1 March until 30 June 2004. There were in general 1-2 Terra MODIS acquisitions per day. Envisat ASAR Wide Swath (WS) images were ordered from 15 April, in average two days a week (some weeks several more). Before this date, all products are based on MODIS alone.

Two parameters were varied in the experiments:

- The time decay function, $conf_{time}(i)$, was set to 0.30, 0.15, and 0.10, which corresponds to a maximum time horizon of 3, 6 and 9 days after the first day. We also studied the effect of using the day products with a 1 day time horizon
- The inter-sensor confidence factors were set to $conf_{INTER-OPT} = 1.0$ and $conf_{INTER-SAR} = 0.75$. We also examined the effect of using results from one sensor only (single-sensor day-products)

We start by looking at a period of products in May 2004 to illustrate how the multi-sensor time-series algorithm works in general. The first day of the period is 9 May and consists of an optical day product and as well as a SAR product. Being the first day in a time series, the day product corresponds to a situation where there have been no useful observations for a while. This situation might appear if there are several days of full cloud cover with only dry snow present in the SAR products. Figure 4.11a shows the optical day product and Figure 4.11b the multi-sensor time-series day product. We see that the mapped area increased by including SAR data, and that the two results appear to agree quite well.

When new day products are added by the multi-sensor time-series algorithm, the mapped area might increase, and the estimated values updated according to the confidence functions. In Figure 4.11c we see the development of the multi-sensor time-series product the first few days after its initiation. The second day in the time series, 10 May, yielded good optical observations, which updated and confirmed the existing data and increased the mapped area to almost the whole mountain region. The next two days were cloudy. Therefore, there was no day product on 11 May and only a SAR day product on 12 May, see Figure 4.11d. On 12 May it is clear that the confidence decay function of time has worked on the existing time-series product. In the western part of the map we see that the SAR product has been applied. Note the difference to the east, where the SAR product had zero confidence and the existing multi-sensor time-series product was decayed below the threshold (the grey colour indicating clouds). The reason for zero radar confidence here may be presence of forests. Also note that some locations near the coast in the west have been wrongly classified as snow in the radar product.

The period 13-22 May continued to be dominated by clouds, and the daily time-series had to rely on old products and radar observations. Figure 4.11e shows the product for 19 May, and almost all the snow-covered mountain areas result from optical data. Some clouds in the

western part are misclassified as snow covered. The SAR products have identified a lot of snow cover, but these areas are surrounded by unclassified pixels. We cannot say from the product whether those areas actually are snow covered or not.

The optical SCA product for 23 May updated and verified the multi-sensor time-series product in the east and south. An important difference, when utilising optical products compared to SAR products, is the ability to estimate fractions of snow cover. The radar SCA gives a more binary result, and often yields a patchy appearance, while the optical data (based on the NLR algorithm) gives a more smooth appearance.

The time-series product of 25 May is shown in two different versions, one with optical data only (Figure 4.11f), and one where also SAR data have been included (Figure 4.11g). The SAR data improves the classification in the northwest by identifying snow-covered areas as well as snow-free areas. Note that in the eastern part of the radar product some strange patches of snow appear within the snow-free areas.

In Figure 4.11h we show the last product for this period. From 27 May the sky was mainly cloud-free for large parts of the area. The last day product of 31 May used here is based on Envisat MERIS data. Since MERIS does not allow detection of clouds over snow-covered surfaces, it is hard to use this sensor operationally. However, this product indicates that SCA retrieval from MERIS works as well as for MODIS.

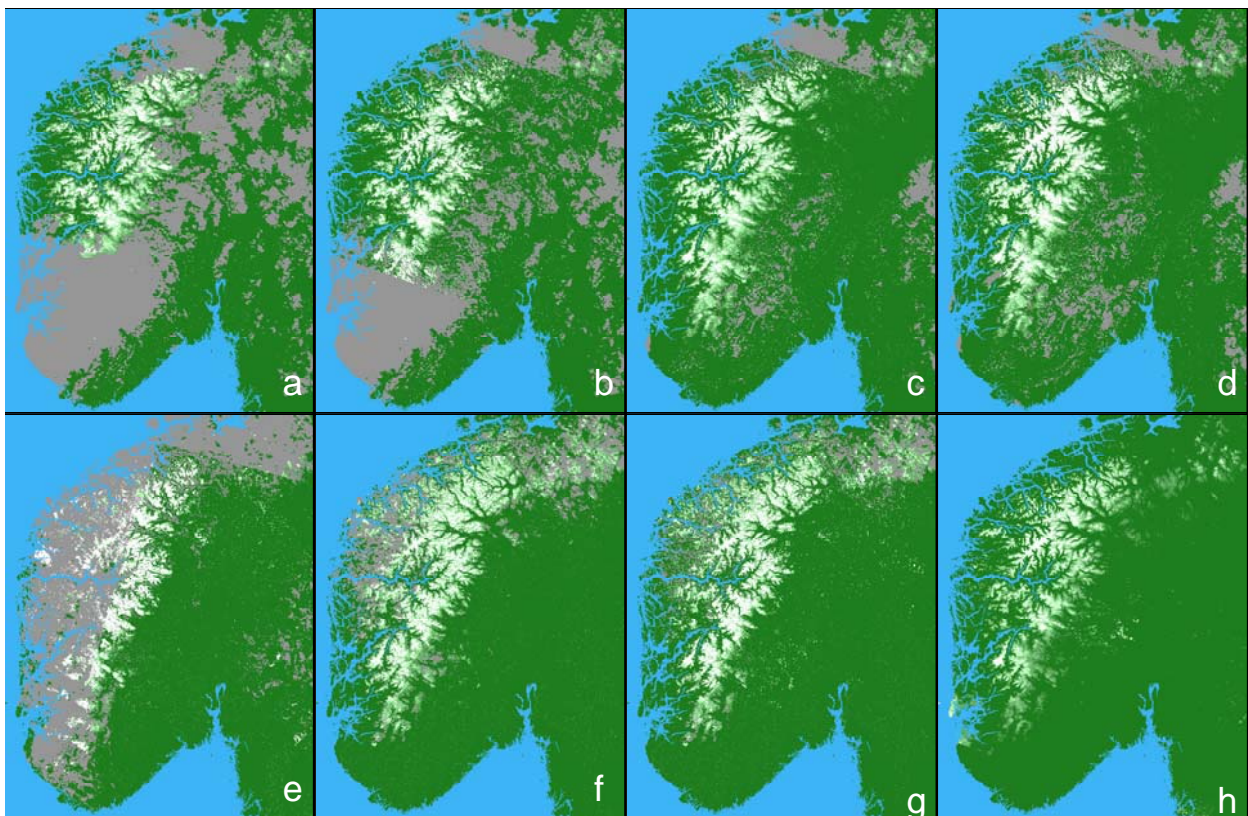


Figure 4.11. Multi-sensor time-series SCA products from May 2004. Fractional snow cover is shown on a scale from green (snow free), via tones of green to white (100% snow cover). Clouds and other areas of zero confidence are shown in grey. When not specified, MODIS and ASAR have been used as the data sources. From upper left: a) Optical product for 9 May 2004; b) Multi-sensor time-series product for 9 May 2004. The product consists of optical observations as well as SAR observations; c) 10 May; d) 12 May; e) 19 May. Most of the mountain areas are mapped from the SAR data. Optical data with cloud mask errors cause false snow in the west and south; f) 25 May, with inclusion of optical data only; g) 25 May, also with inclusion of SAR data; h) 31 May, single-image product where MERIS has here been used as the data source (without cloud masking).

A single sensor or day product will not give SCA values for the whole area. This is caused by cloud coverage and radar-shadow effects. One measure of quality of an SCA product is the total area covered by observations. We have calculated the area covered in percent of the total land area (South Norway) for day products, single-sensor products and single-sensor time-series products. This has been done for all combinations of confidence parameters.

In Figure 4.12 the area with SCA data in percent of the total area is shown for different multi-sensor time-series products for each day throughout the test period. Both inter-sensor confidence factors are set to 1.0. The plot shows how the coverage varies with the time horizon.

Figure 4.13 shows the coverage of SCA data for multi-sensor time-series products with two values of the inter-sensor confidence factor for the test period. We see little difference for the values 1.0 and 0.75. Both give a better coverage than a single-sensor MODIS time-series product.

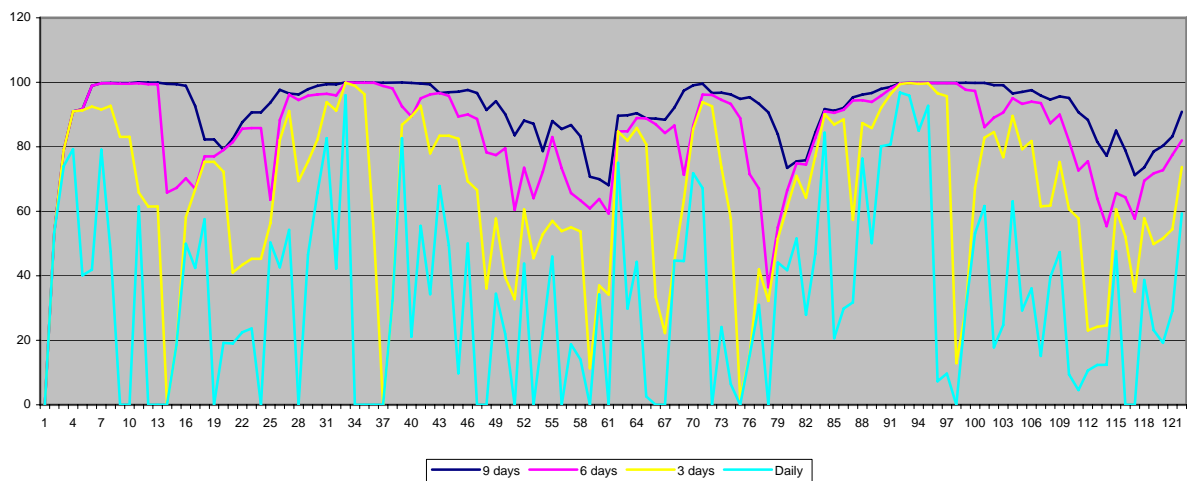


Figure 4.12. Data coverage in percentage of the total land area for multi sensor products with different time horizons. The inter-sensor confidence factor is 1.0 for both sensors

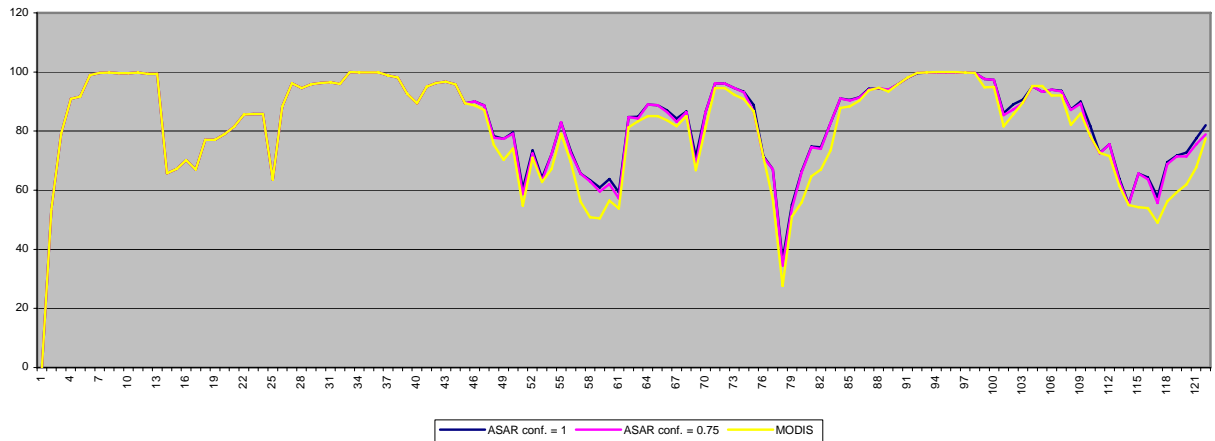


Figure 4.13. SCA coverage in percentage of the total area for two values of the inter-sensor confidence factor. A time-series MODIS product is also shown

Mean values for the coverage through the test period of 122 days are given in Table 4.5. Coverage for an ASAR single-sensor time-series product is not calculated because it is not directly comparable to the other alternatives. Forested areas are masked out for SAR. In the SAR product this is shown as zero confidence in the forested areas. The SAR product also gives confidence zero for lakes and for the area inside Sweden. Therefore, the calculated area of SCA values for ASAR will always be much less than for MODIS.

Figure 4.14 illustrates in more detail the differences between the results of SCA retrieval from optical data and SAR data. Six days time horizon and an inter-product confidence factor of 1.0 were applied. In this time-series multi-sensor product of 7 June 2004, ASAR data has yielded a more binary looking product. Lots of partly snow-covered areas disappear by including ASAR, probably due to backscatter from patches of snow-free ground this late in the snowmelt season.

Table 4.5. Mean coverage of the land area in percentage for a MODIS time-series product and multi-sensor time-series day products with different time horizons and inter-sensor confidence factors

	1 day	3 days	6 days	9 days
MODIS		61.48	81.21	89.38
<i>conf</i>_{INTER-SAR} = 1.0	33.14	64.68	83.76	91.11
<i>conf</i>_{INTER-SAR} = 0.75	33.14	64.18	83.39	90.92

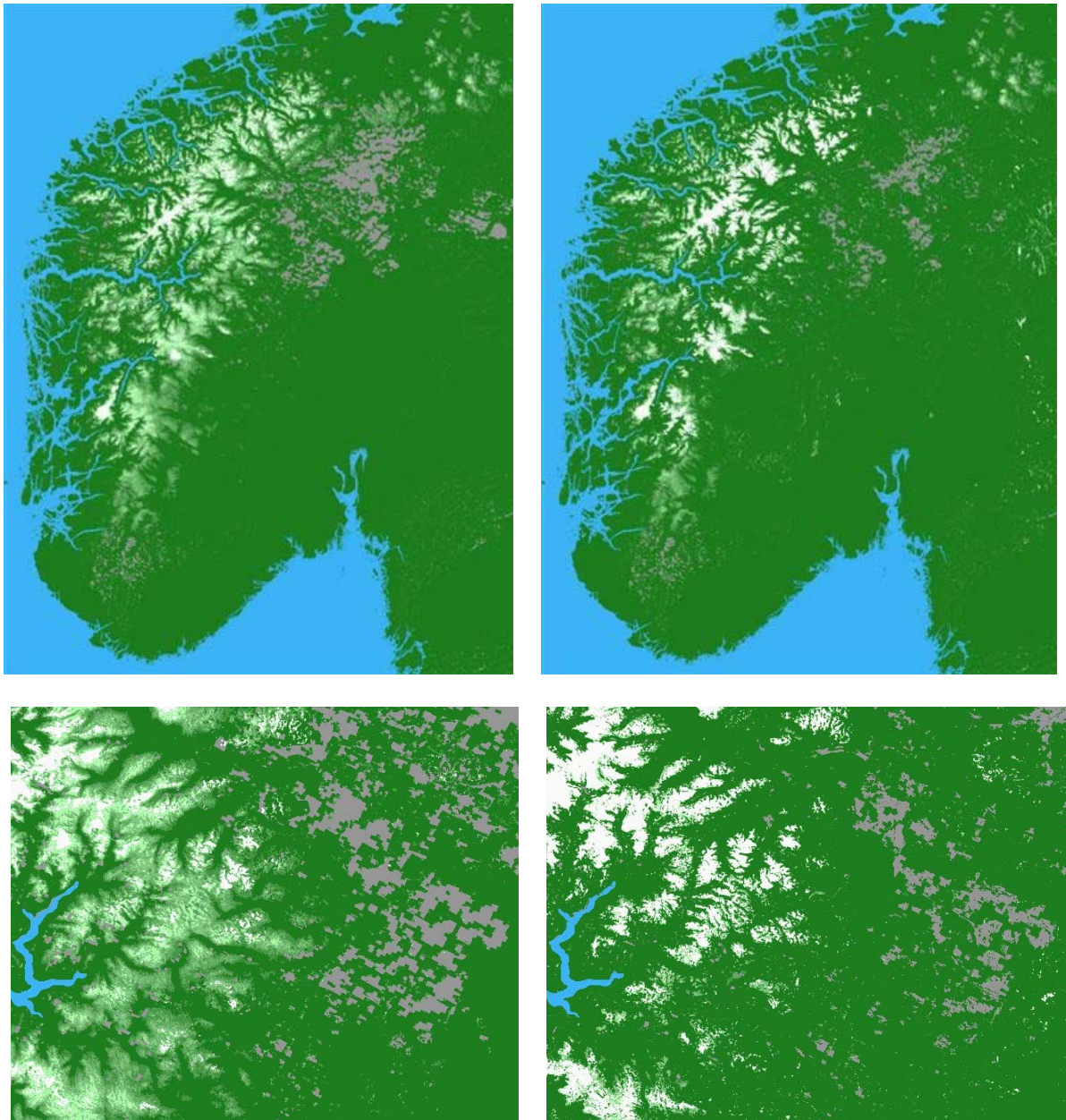


Figure 4.14. The day product with and without ASAR on 7 June 2004. Left: MODIS only included. Right: Both MODIS and ASAR included. Top: Overview of South Norway. Below: Enlargement of the Jotunheimen area. After the inclusion of ASAR data the SCA tends to approach the extreme values of 0% and 100% and lots of snow seems to have disappeared. In other places the snow cover appears to have increased from partial to complete coverage.

5 Discussion of results

The results from the experiments presented in the previous chapter are discussed here. Brief conclusions are made for each of them, while further discussion and recommendations for operational use is left to the next chapter.

5.1 The NLR algorithm

The performance of the NLR algorithm was studied in the previous chapter by comparison of snow maps based on Landsat images and MODIS snow maps based on the NLR algorithm. As seen in the examples, there were large uncertainties associated with the SCA estimates from the Landsat images. It varies from image to image with minimum variation for 2003.03.01 (97.47–99.33%) and maximum for 2004.05.23 (45.98–70.24 %) and 2004.05.30 (37.44–59.43). The main reason for the difference in uncertainty lies in the snow distribution. In the image from 2003.03.01 the area is totally covered with snow. There are just some very steep hillsides without snow. The problem with shadows has been solved, so most of the snow in the shaded areas has been detected. In the other images the snow has started melting, and there are large and small patches of snow, which complicates the classification. We have the problem of pixels partly covered with snow, and old snow with low reflectance. For 2004.05.30 the snow fragmentation was extensive, so the number of pixels with uncertain amount of snow was very large. For 2004.05.23 the classification resulted in some classes where large areas were completely covered with snow and small areas in the same class were obviously only partly covered. Assuming 50% coverage for these classes probably gives a too small value for the mean SCA value.

Compared to the SCA maps based on Landsat, the NLR algorithm used on MODIS images underestimates the amount of snow in all cases. Except for 2004.05.23 and 2004.05.30 the derived SCA is even below the minimum Landsat values for all images.

The estimated SCA from MODIS was compared with the calculated mean value for Landsat. Remember that this is not an exact value of the snow cover area, but an estimate with an amount of uncertainty, which is hard to specify. We see that the estimated SCA varies from 45.95 % to 92.90% of the estimated 'correct' value. The value of 92.90% is probably far too high. The estimated mean SCA value of 2004.05.23 from the Landsat image is very uncertain. As we do not know the correct value, we cannot say for sure that the result from 2004.05.23 is better than 2003.04.18 or 2005.05.30.

There are good explanations for the low estimates:

Topography: The NLR algorithm does not take into account the topography of the scene. From slopes facing away from the sun the reflected radiation received at the satellite will be lower than from horizontal areas and slopes facing towards the sun. The calibration areas with 100% snow coverage are situated on the top of glacier plateaus, and are horizontal in the average. This means that for areas with 100% snow cover facing away from the sun, the estimated snow cover in many cases will be less than 100%. This effect is most visible in the winter when the sun is not high above the horizon. With low sun there will also be large shadows in mountainous areas. This may result in estimation of no snow in shadowed areas even if the real snow cover is 100%.

Snow age: Newly fallen snow has a very high reflectance. The snow grain size increases and the reflectance decreases with time. The snow will also be polluted by particles from bare ground and vegetation. This is particularly effective near the edges of snow patches late in the melting season. In the summer the snow fallen last winter may melt totally, and old snow from earlier years may appear. This snow is especially dirty with very low reflectance. When the snow melts on glaciers, ice with low reflectance may appear. These effects lead to underestimates of snow cover late in the melting season.

Bare ground surface type: The NLR algorithm handles the two-class problem of spectral unmixing where the reflectance values of the two classes are determined by transformations of the reflectance values of the calibration areas. In practice the surface reflectance varies a lot, and some classes may easily result in FSC > 0% even when the ground is snow free. Also, small snow-patches left in the calibration areas for snow-free ground might not be detected and will therefore create errors in the reflectance-to-FSC transformation.

The geometrical correction algorithm seems to work well in most cases with MODIS scenes with resolution of 250 m. Most of the images in this study have been geometrically corrected to the used projection with errors of 250 m or less. For a couple of images the errors were found to be about 2 pixels (500 m), perhaps as much as 3 pixels (750 m) in some areas. The geometrical correction has been studied inside the validation area only.

5.2 The cloud detection algorithm

Selected snow maps have been compared with the MOD35_L2 MODIS cloud mask product provided by NASA. As a rule, the KNN-classifier based method produces a better cloud mask than the MODIS cloud mask product. There are small differences in general, but the main difference lies in detection of clouds over and at the borders of snow-covered areas. MOD35 frequently shows clouds along most of the edges of the snow covered area. In some cases the KNN classifier also produces a few extra clouds near the snow edges, but it is considered as a minor problem. In cases with cold weather and dry snow, the MOD35 product could show clouds over large snow covered areas when there are no clouds. This problem has been practically removed in the KNN-classifier, but we have seen cases where clouds have been incorrectly detected over small areas with cold snow where there are mainly wet snow in the surroundings.

The MOD35 algorithm has been developed for global applications for all types of clouds all over the Earth in all seasons. NR's algorithm has on the other side been tailored for the snowmelt season in Norway. Therefore, it could be expected to produce generally better results under these conditions. Using different codebooks for the different seasons (winter, spring and summer) may further improve the cloud detection.

Close studies of the results from generation of time series of SCA products by the NLR algorithm show that in some cases clouds over snow-free land have not been detected. The cloud pixels are classified as snow and give a wrong value of the snow coverage. Cloud shadows can also reduce the estimated SCA value.

There are some difficulties with cloud labelling in the training process of the algorithm. There are two main types of clouds – transparent and opaque clouds. If the thin transparent clouds are labelled as clouds, the classification algorithm will probably detect them as clouds and they will be included in the cloud mask. When aiming at mapping the snow cover, one might try to neglect these clouds because the ground below is visible. But the clouds will reduce the reflected light from the snow, and one might end up with incorrect values for the snow cover percentage. When labelling, it is often difficult to see if there are thin clouds or not. One could probably use more than one cloud class and separate the opaque from the transparent clouds. If the classification procedure manages to discriminate the two types of clouds, one might be able to detect the snow also in areas with thin clouds. But one should then reduce the confidence of the results in such areas.

5.3 NR's new optical snow model algorithm

Even if the contrast between snow and snow-free ground is quite high in general, accurate mapping of the snow cover is not straightforward. This is partly due to the situation that the snow fraction at the sub-pixel level is needed to obtain the required level of detail for the snow maps. Combined with the fact that the snow spectrum changes continuously and that the regions to monitor frequently has complex terrain relief, this has resulted in a failure to obtain very accurate operational fractional snow cover monitoring for larger regions under all snow conditions.

For smaller regions, high accuracy has been obtained at the sub-pixel level by a few authors (like in Painter et al., 2003). It is characteristic for such experiments that detailed knowledge and models have been established for the region at hand. For large-scale mapping, it is practically hard to apply the same approaches.

The approach taken here is to avoid using detailed local ancillary data and complex physical models, and instead deriving local information from time series of measurements to establish and parameterize empirical models. This makes it feasible to apply the method on larger regions. However, a data assimilation period is required to build up the necessary local models.

The limited experiments performed so far with the new approach confirm that significantly higher accuracy, compared to classical, operational approaches (e.g. NLR), is achievable. Errors seem to deviate with less than 5% from SCA in the reference data (Landsat TM and aerial images) for regions with terrain relief and snow states where classical methods typically give large errors. If the high accuracy can be proved to be valid in general, the method should be attractive for local applications (like hydropower hydrology) as well as for global applications (like climate change monitoring) where high accuracy is a requirement.

Future plans include large-scale validation for a variety of snow states and adaptation of the method to snow monitoring in forested regions.

5.4 Multi-sensor time-series snow cover algorithm

The current results for the day-product version of the multi-sensor time-series algorithm show that the products depend very much on how the initial single-sensor product confidence is set and on the time decay function. It appears that closeness to clouds should have been given reduced confidence in the optical data in order to reduce the risk of classifying clouds as snow. More important, however, is to consider how to fuse the SAR and optical data better.

When optical data are unavailable due to clouds, the use of radar data improves the product by covering larger areas. Due to the binary character of the radar snow map and the limitation to detect wet snow only, we set the inter-product confidence factor for SAR to a lower value than for optical in some of the experiments. We examined and evaluated various inter-product confidence factors for SAR, and we found that factors of 0.5 and below clearly reduced the contribution from the SAR products too much. Using a value close to 1.0 preserves much of the binary pattern from the ASAR products. This means that high confidences for SAR had a tendency to override subsequent optical products. We found that values in the range 0.75-1.0 gave the best overall results.

We examined the effect of including assumptions about dry snow in the radar product. Using a SAR SCA product including also inferred dry snow (above the wet-snow zone in mountainous areas) appeared to overestimate the snow cover compared to the optical product. Using SAR SCA based on wet snow only appeared to underestimate the snow cover compared to the optical product. We also tried to reduce the confidence of SAR pixels classified as dry snow, but this did not improve the result significantly.

Based on the experiences from all the runs of the algorithm we found that 6 days time horizon was optimal for the cases we tested. While 3 days resulted in too many unclassified pixels, the 9 days runs resulted in marginal improvements in coverage and too many old observations in periods of rapidly changing SCA. We did not find any significant difference between the two inter-product confidence factors in our tests. It was clearly better to use the combination of two sensors than a single-sensor approach.

Some experiments were performed with MERIS data instead of MODIS. The MERIS-based single-scene SCA maps seem to be of similar quality as the MODIS-based maps for cloud-free conditions. However, clouds make serious problems over snow-covered surfaces since MERIS does not have the spectral bands needed to separate snow and clouds spectrally. AATSR can be used for generating a cloud mask, but it would, unfortunately, only cover a part of the MERIS scene. If one limits the use of the MERIS image to the area covered by AATSR, less frequent coverage would be a consequence.

We also tested an approach where the SCA values of the best single-sensor optical and SAR products were combined as a weighted mean of the two. The weights used were proportional to the confidence of the corresponding pixels. The approach did not change the product very much in general. When the SCA values of optical and SAR differed much, the result had a tendency to be worse (one of the values might be an "outlier", then worsening the "good" value).

Other approaches of combining optical and SAR could be considered. Instead of combining the two sensors when making a day product, we could leave the day product idea and combine ASAR with an updated time-series product (which already has included the current MODIS

day product). However, any approach where we use weighted mean to update the time series will make it difficult to control how long time one observation should be allowed to influence the time series.

A better idea could be to maintain two independent time series, one for each sensor and updated by the "selection-of-best" approach. For each day any relevant algorithm can now be applied in order to retrieve the combined product, without pushing this multi-product forward and influencing the future products. A more general approach would be to store all observations for at least the defined time horizon, and then reanalyse all data for each multi product that is going to be produced.

It is obvious that the confidence of the combined product should depend on how well the two inputs match each other. If two independent observations confirm each other, the confidence should be increased. If they contradict each other, the confidence should be reduced.

6 Overall conclusions and recommendations

This chapter provides the main conclusions for the Norwegian optical algorithms presented in the report and some considerations when comparing the algorithms. Furthermore, overall conclusions from the review of the internationally available algorithms are provided, and the results are compared to those obtained with the Norwegian algorithms. Finally, two scenarios for operational national-wide applications for snow monitoring are presented.

6.1 Norwegian algorithms

NLR: The overall conclusion for the NLR algorithm is that the snow cover area is somewhat underestimated in general. However, it is hard to conclude quantitatively, from experiments comparing SCA retrieved from MODIS images using NLR with SCA maps based on Landsat TM and ETM+, exactly how large the underestimation is. The underestimation is especially noticed in mountainous regions. In winter and early spring, there will be shadows because of the low sun. There will also be underestimation of snow in slopes facing northerly. These errors will decrease as the sun rises higher. The best results are obtained in April and May before significant fragmentation and pollution of the snow occurs. In this period the algorithm gives satisfying results with accuracy of 80-90%. Towards the summer the underestimation will increase because of dirty snow.

Clouds: NR's cloud algorithm has been found to work quite well over Norway, and generally better than NASA's algorithm for the MOD35_L2 MODIS cloud mask product. There are small differences in general, but the main difference lies in detection of clouds over and at the borders of snow-covered areas. MOD35 frequently shows clouds along most of the edges of the snow covered area. In cases with cold weather and dry snow, the MOD35 product could show clouds over large snow-covered areas when there are no clouds. NR's cloud algorithm is sometimes not able to detect clouds over snow-free land and classify these pixels as snow. Cloud shadows can also reduce the estimated SCA value.

NR's new optical snow modelling algorithm: This algorithm, currently under refinements and validation, is based on an approach compensating for the deficits of the NLR algorithm. The new algorithm uses local spectral information instead of overall spectral values for bare ground and full snow cover. The local spectral information is represented in an empirical model calibrated with remote sensing data acquired under full snow cover and snow-free conditions. Images are acquired under variable illumination and acquisition angles for establishing a partial BRDF model. The BRDF model makes it possible to compensate for terrain relief as well as variable solar elevation. Also, metamorphosis and impurity models for the development of the reflectance of the snow throughout the snowmelt season make further compensation for errors seen when applying NLR. Preliminary results indicate that errors < 5% could be expected, but this remains to be verified for much larger data sets in space and time.

Multi-sensor time-series algorithm: This algorithm utilises a time series of data from optical and SAR sensors. The algorithm combines the best features of the SAR and optical sensors recognising that optical data are limited by cloud cover and SAR data are limited to wet snow. The algorithm also utilises the information in satellite images much better by using a dataset acquired over time. There is certainly a very strong correlation between neighbouring images in the time series, and this is utilised by also retrieving information from past images when there

are no current observations or the past observations are better for some reason (e.g. less oblique observations in the past). The algorithm fuses the time series of optical and SAR observations using an approach based on confidence functions. The approach ensures that the best possible snow map is generated, given the available data set. Currently, the fusion is taking place at the geophysical level using the best available single-sensor algorithms.

Various versions of the NLR algorithm have been applied operationally for almost two decades. The algorithm has proven to be reasonably robust and as good as or better than other available algorithms (e.g. NASA's MODIS snow algorithm). But better accuracy should be achievable, and NR's new FSC algorithm seems to be far more accurate and robust. However, 1-2 years of refinements and large-scale validation will be needed before it can be used operationally.

A multi-sensor time-series approach has been proven to give significantly better coverage in space and time than using a single-sensor approach. The current confidence-based approach has been tested for a few snowmelt seasons and thereby demonstrated to work very well with respect to coverage in space and time. This is the only way of providing close to daily snow cover maps throughout the whole snowmelt season. However, there is still a lack of harmonisation of the results coming from optical and SAR sensors. The two sensor types observe different geophysical phenomena and, therefore, cannot be expected to give fully consistent results. A new fusion model combining data closer to the physical retrieval process level is currently under development by NR and NORUT IT, but is not expected to be available shortly due to rather limited R&D resources available currently. Anyway, products from the current algorithm represent a significant improvement forward compared to single-sensor products.

6.2 Other algorithms

For operational applications, the above approaches have various drawbacks. The algorithm in Solberg and Andersen (1994) actually assumes that all snow-free ground has the same reflectance. This is certainly not true. At the basin level, and for areas above the tree line, local variations may to some degree cancel out. However, there are also large-scale variations between basins that are not compensated for (one image with one calibration covers several basins).

The spectral unmixing approach compensates for this problem by decomposing more than two spectra, hopefully all endmembers in the scene. The original algorithm in Nolin (1993) has the problem of being supervised. The problem was solved in Rosenthal (1996) by including a spectral library, and the approach was further improved in Painter et al. (2003). However, it is practically impossible to have all snow reflectance classes available in a library since the snow spectral reflectance, and specifically the BRDF, develops continuously due to snow crystal metamorphosis and contamination by impurities.

Another and more general problem with spectral unmixing is that there will usually be, in particular with a high number of possible endmembers, many solutions to the set of linear equations to be solved. Hence, the high variability of the snow reflectance will with the above approaches of spectral unmixing necessarily give variable accuracy, in particular during the

snowmelt season. These problems are handled in the new approach proposed in Solberg 2004 and 2005.

Other approaches for FSC retrieval have also been published. Salomonson and Apple (2004) tested whether there was enough “signal” in NDSI to map fractional snow, and they identified a linear relationship between FSC and NDSI. A MODIS FSC product is currently launched. Kaufman et al. (2002) developed an algorithm for retrieval of fractional snow cover based on an approach derived from remote sensing of aerosols over varying terrain. The algorithm works best for lower FSC levels. Simpson and McIntire (2001) tested two types of neural networks to estimate fractional snow cover. A feed-forward neural network was used to classify individual images, while a recurrent neural network was used to classify sequences of images. A method for mapping snow cover fraction at the basin level in forested areas has been proposed by Metsämäki et al. (2005). Snow maps are generated for the entire Finland using this method. Vikhamar and Solberg (2003b) propose a spectral unmixing approach using of a land-cover map to constrain the unmixing.

As far as it is possible to compare the published algorithms, based on results from analysing different data sets, it seems reasonable to conclude that the spectral unmixing approach gives overall best results. Spectral unmixing has been used in various ways by different authors. The best results are usually obtained when ancillary information is included in the retrieval process, such as a library of spectral signatures and land-cover maps.

6.3 Operationalisation scenarios

Based on the available algorithms and algorithms currently under development, two scenarios for operationalisation are provided – one conservative and one offensive:

Scenario I: If an operational algorithm is needed immediately:

- *Step 1:* Start using NLR, which is proven and has well-known characteristics
- *Step 2:* Convert to NR’s new optical algorithm when this is available in 1-2 years
- *Step 3:* Switch to a new multi-sensor time-series approach utilising both SAR and optical data, which should be available in 2-4 years

Scenario II: Operation is started in two years:

- *Step 1:* Assuming that a sound R&D project is funded for the next 2 years, complete the validation and refinements of NR’s new algorithm and in parallel develops a sound multi-sensor fusion approach. New single sensor algorithms are applied in the multi-sensor fusion approach and again combined with the current confidence-based time-series approach
- *Step 2:* Use the new multi-sensor time-series algorithm for the operational application

Scenario I represents a conservative and defensive approach where one in any case can fall back to the previous (current) solution if the next solutions fails or is delayed. However, the quality will be limited for the first 1-2 years and the coverage in space and time will be limited over 2-4 years due to the limitation set by clouds for optical sensors. Daily observations can be expected available only after up to 4 years.

Scenario II represents a more aggressive approach with parallel work on single sensor and multi-sensor algorithms. As the new optical single-sensor algorithm is closer to finalisation, it should be available in time for integration with a new multi-sensor fusion approach when the first baseline version is available after approximately 1 year. The new algorithm should be available already after 2 years if the R&D project is of sound size.

Note that Scenario I is based on the assumption that some (but not very much) funding is available for development and validation. Currently, only a very small amount of internal funding is secured for the next couple of years.

7 References

- Andersen, T. (1982). "Operational snow mapping by satellites." *Proceedings of the Exeter symposium*, July 1982, IAHS publ. no. 138, 1982, pp. 149-154.
- Bailey, J.O., Barrett, E.C., Beaumont, M.J., Herschy, R.W., Kelly R.E.J. and Xu H. (1993). *Remote Sensing of Snow by Satellite*. Research Report, R&D Project 207, Remote Sensing Unit, University of Bristol.
- Baumgartner M.F. and Rango A. (1995). "A microcomputer-based alpine snow-cover analysis system (ASCAS)." *Photogrammetric Engineering & Remote Sensing*, Vol. 61, No. 12, pp. 1475-1486.
- Dozier, J. (1989). "Spectral signature of alpine snow cover from the Landsat Thematic Mapper." *Remote Sensing of Environment*, 28, 9-22, 1989.
- Duda, R.O., Hart, P.E. and Stork, D.G. (2001). *Pattern Classification*, John Wiley & Sons, Inc., 2001.
- Ferner, S. and Sutherland, I. (1987). "The utility of computer-processed NOAA imagery for snow cover mapping and streamflow simulation in Alberta." *Proceedings of the Vancouver symposium*, August 1987, IAHS publ. no. 166, pp. 173-184.
- Fily, M., Bourdelles, B., Dedieu, J.P. and Sergent, C. (1997). "Comparison of In Situ and Landsat Thematic Mapper Derived Snow Grain Characteristics in the Alps." *Remote Sensing of Environment*, Vol. 59, 1997, pp. 452-460.
- Hall, D.K., Riggs G.A. and Salomonson, V.V. (1995). "Development of methods for mapping global snow cover using Moderate Resolution Imaging Spectroradiometer (MODIS) data." *Remote Sensing of Environment*, vol. 54, pp. 127-140, 1995.
- Harrison, A.R. and Lucas, R.M. (1989). "Multi-spectral classification of snow using NOAA AVHRR imagery." *International Journal of Remote Sensing*, Vol. 10, pp. 907-916.
- Huseby, R.B., Halck O.M. and Solberg R. (2005). "A model-based approach for geometrical correction of optical satellite images." *International Journal of Remote Sensing*, No. 15, Vol. 26, pp. 3205-3223, 1 August 2005.
- Kaufman, Y.J., Kleidman, R.G., Hall, D.K. and Martins, J.V. (2002). "Remote sensing of subpixel snow cover using 0.66 and 2.1 μm channels." *Geophysical Research Letters*, vol. 29, no. 16, 2002.
- Klein, A.G. Hall D.K. and Riggs G.A. (1997). "Improving the MODIS global snow-mapping algorithm." *Proceedings of the International Geoscience and Remote Sensing Symposium (IGARSS 1997)*, 4-8 August 1997, Singapore, pp. 619-621.
- Koskinen, J., Metsämäki, S., Grandell, J., Jänne, S. Matikainen, L. and Hallikainen M. (1999). "Snow Monitoring Using Radar and Optical Satellite Data." *Remote Sensing of the Environment*, vol. 69, pp. 16-29.
- Metsämäki, S.J., Anttila, S.T., Markus, H.J. and Vepsäläinen (2005). "A feasible method for fractional snow cover mapping in boreal zone based on a reflectance model." *Remote Sensing of Environment*, Vol. 95, 2005, pp. 77-95.
- Myers, W.L. and Patil, G.P. (2006). *Pattern-Based Compression of Multi-Band Image Data for Landscape Analysis*, Springer, 2006.
- Nagler, T. and Rott, H. (2000). "Retrieval of wet snow by means of multitemporal SAR data", *IEEE Trans. Geoscience and Remote Sensing*, vol. 38, pp. 754-765, 2000.
- Nolin, A.W. and Dozier, J. (1993). "Estimating snow grain-size using AVIRIS data." *Remote sensing of environment*, 44 (2-3): 231-238.
- Painter, T.H., Roberts, D.A., Green, R.O. and Dozier, J. (1998). "The effect of grain size on spectral mixture analysis of snow-covered area from AVIRIS data." *Remote Sensing of Environment*, Vol. 65, 1998, pp. 320-332.
- Painter, T.H., Dozier, J., Roberts, D.A., Davis R.E. and Green, R.O. (2003). "Retrieval of subpixel snow-covered area and grain size from imaging spectrometer data." *Remote Sensing of Environment*, Vol. 85, 2003, pp. 64-77.
- Raggam, J., Almer A. and Strobl D. (1994). "A combination of SAR and optical line scanner imagery for stereoscopic extraction of 3-D data." *Journal of Photogrammetry and Remote Sensing*, vol. 49, no. 4, pp. 11-21.
- Riggs, G.A. Hall D.K. and Salomonson V.V. (1994). "A snow index for the Landsat Thematic Mapper and Moderate Resolution Imaging Spectroradiometer." *Proceedings of the International Geoscience and Remote Sensing Symposium (IGARSS 1994)*, 8-12 August 1994, Pasadena, California, USA, pp. 1942-1944.

- Riggs, G.A. Hall D.K. and Salomonson V.V. (1996). "Recent progress in development of the Moderate Resolution Imaging Spectroradiometer snow cover algorithm and product." *Proceedings of the International Geoscience and Remote Sensing Symposium (IGARSS 1996)*, Lincoln, NE, pp.139-141, 1996.
- Ripley, B.D. (1996), *Pattern Recognition and Neural Networks*, Cambridge University Press.
- Rosenthal, W. (1996). "Estimating alpine snow cover with unsupervised spectral unmixing." *Proceedings of the International Geoscience and Remote Sensing Symposium (IGARSS 1996)*, 27-31 May 1996, Lincoln, Nebraska, USA, pp. 2252-2254.
- Rosenthal, W. and Dozier J. (1996). "Automated mapping of montane snow cover at subpixel resolution from the Landsat Thematic Mapper." *Water Resources Research*, Vol. 32, No. 1, pp. 115-130.
- Salomonson, V.V. and Apple, I. (2004). "Estimating fractional snow cover from MODIS using the normalized difference snow index." *Remote Sensing of Environment*, Vol. 89, 2004, pp. 351-360.
- Salomonson, V.V. and Apple, I. (2006). "Development of the Aqua MODIS NDSI fractional snow cover algorithm and validation results." *IEEE Transactions of Geoscience and Remote Sensing*, vol. 44, no. 7, July 2006.
- Simpson, J.J. and McIntire, T.J (2001). "A recurrent neural network classifier for improved retrievals of areal extent of snow cover." *IEEE Transactions of Geoscience and Remote Sensing*, vol. 39, no. 10, October 2001.
- Solberg, R. (2004). "A high-precision dynamic and adaptive BRDF and fractional snow-cover monitoring algorithm." *Proceedings of IEEE International Geoscience and Remote Sensing Symposium (IGARSS 2004)*, Anchorage, Alaska, USA, September 20, 2004.
- Solberg, R. (2005). "Model-Driven Retrieval of Fractional Snow Cover Area." *Proceedings of IEEE International Geoscience and Remote Sensing Symposium (IGARSS 2005)*, Seoul, Korea, 25-29 July 2005.
- Solberg, R, Amlien, J., Koren, H., Eikvil, L., Malnes E. and Storvold, R. (2004a). "Multi-sensor and time-series approaches for monitoring of snow parameters." *Proceedings of IEEE International Geoscience and Remote Sensing Symposium (IGARSS 2004)*, Anchorage, Alaska, USA, 20-24 September 2004.
- Solberg, R, Amlien, J., Koren, H., Eikvil, L., Malnes E. and Storvold, R. (2004b). "Multi-sensor/multi-temporal analysis of ENVISAT data for snow monitoring." *ESA ENVISAT & ERS Symposium 2004*, Salzburg, Austria, 6-10 September 2004.
- Solberg, R, Amlien, J., Koren, H., Eikvil, L., Malnes E. and Storvold, R. (2005). "Multi-sensor/multi-temporal approaches for snow cover area monitoring." *Proceedings of EARSeL LIS-SIG Workshop*, Berne, February 21-23, 2005.
- Solberg R. and Andersen, T. (1994). "An automatic system for operational snow-cover monitoring in the Norwegian mountain regions." *Proceedings of the International Geoscience and Remote Sensing Symposium (IGARSS 1994)*, 8-12 August 1994, Pasadena, California, USA, pp. 2084-2086.
- Storvold, R., Malnes, E. and Lauknes, I. (2006). "Using ENVISAT ASAR wide-swath data to retrieve snow covered area in mountainous regions." *EARSeL eProceedings*, 4(2), 150-156, 2006.
- Swamy A.N. and Brivio P.A. (1996). "Hydrological modelling of snowmelt in the Italian Alps using visible and infrared remote sensing." *International Journal of Remote Sensing*, Vol. 17, No. 16, pp. 3169-3188.
- Tait, A.B., Hall, D.K., Foster, J.L. and Armstrong R.L. (2000). "Utilizing Multiple Datasets for Snow-Cover Mapping." *Remote Sensing of the Environment*, vol. 72, pp.111-126.
- Tampellini, M.L., Brivio, P.A., Carrara, P., Fantoni, D., Gnocchi, S., Ober, G., Pepe, M., Rampini, A. Ratti, R., Nodari F.R. and Strozzi T. (2004). "Monitoring snow cover in alpine regions through the integration of MERIS and AATSR ENVISAT satellite observations." *Proceedings of MERIS User Workshop*, Frascati, Italy, 10-13 November 2003 (ESA SP-549, May 2004).
- Vikhamar, D. and Solberg, R. (2003a). "Snow-cover mapping in forest by constrained linear spectral unmixing of MODIS data." *Remote Sensing of Environment*, vol. 88 (2003), pp. 309-323.
- Vikhamar, D. and Solberg, R. (2003b). "Subpixel mapping of snow cover in forest by optical remote sensing." *Remote Sensing of Environment*, vol. 84 (2003), pp. 69-82.
- Vikhamar, D., Solberg, R. and Seidel, K. (2004). "Reflectance modeling of snow-covered forests in hilly terrain." *Photogrammetric engineering and remote sensing*, vol. 70 (2004), no. 9, pp. 1069-1079.
- Warren S.G. and Wiscombe, W.J. (1980). "A model for the spectral albedo of snow, II, Snow containing atmospheric aerosols," *Journal of Atmospheric Sciences*, Vol. 37, 1980, pp. 2734-2745.
- Wiscombe W.J. and Warren S.G. (1980). "A model for the spectral albedo of snow, I, Pure snow," *Journal of Atmospheric Sciences*, Vol. 37, 1980, pp. 2712-2733.

- Xu, H., Bailey, J.O., Barrett E.C. and Kelly R.E.J. (1993). "Monitoring snow area and depth with integration of remote sensing and GIS." *International Journal of Remote Sensing*, Vol. 14, pp. 3259-3268.
- Østrem, G., Andersen T. and Ødegaard, H. (1979). "Operational use of satellite data for snow inventory and runoff forecasting." *Proceedings of the Pecora Symposium*, American Water Resources Association, June 1979, pp. 230-234.

